CHALMERS
UNIVERSITY OF TECHNOLOGY

Chemical Looping Combustion Of Solid Biomass in Packed-Fluidized Bed Reactor

An Experimental Investigation of Reactor Performance

Master's thesis in Sustainable Energy Systems

Saeid Davam

DEPARTMENT OF ENVIRONMENTAL AND ENERGY SCIENCES

CHALMERS UNIVERSITY OF TECHNOLOGY
Gothenburg, Sweden 2026
www.chalmers.se

Master's thesis 2026

Chemical Looping Combustion of Solid Biomass in a Packed-Fluidized Bed Reactor

An Experimental Investigation of Reactor Performance

SAEID DAVAM

CHALMERS
UNIVERSITY OF TECHNOLOGY

Department of Environmental and Energy Sciences
Chalmers University of Technology
Gothenburg, Sweden 2026

Chemical Looping Combustion of Solid Biomass in a Packed-Fluidized Bed Reactor
An Experimental Investigation of Reactor Performance

SAEID DAVAM

© SAEID DAVAM, 2026.

Supervisor: Nasrin Nemati, Department of Environmental and Energy Sciences
Examiner: Magnus Ryndén, Department of Environmental and Energy Sciences

Master's Thesis 2026
Department of Environmental and Energy Sciences
Chalmers University of Technology
SE-412 96 Gothenburg
Telephone +46 31 772 1000

Chalmers Digital Print
Gothenburg, Sweden 2026

Chemical Looping Combustion of Solid Biomass in a Packed-Fluidized Bed Reactor

SAEID DAVAM
Department of Environmental and Energy Sciences
Chalmers University of Technology

Abstract

Chemical Looping Combustion (CLC) is a promising carbon capture technology that inherently separates CO_2 during combustion, reducing the need for energy intensive gas separation. A key limitation of conventional fluidized bed CLC reactors is that at higher gas velocities, bubble size increases, which reduces gas–solid mass transfer and limits fuel conversion efficiency. This study investigates the effect of introducing packed materials into a fluidized bed CLC reactor forming a Packed-Fluidized Bed Reactor (PFBR) to address this limitation.

Batch experiments were conducted in a laboratory-scale reactor at 900°C using ilmenite as the oxygen carrier. Two biomass fuels were tested: wood pellets and torrefied wood pellets. Two packing materials were evaluated: random metal-thread saddle ring (RMSR) and expanded clay aggregate (ECA). Experiments were performed at superficial gas velocities of 0.15 m/s and 0.3 m/s, and fuel conversion performance was assessed through CO_2 yield calculations based on carbon mass balances.

The results show that both packing materials significantly improve CO_2 yield compared to the unpacked configuration. For wood pellets at 0.15 m/s, the average CO_2 yield increased from 73.0% without packing to 91.8% with RMSR and 88.3% with ECA. Torrefied wood pellets consistently achieved higher CO_2 yields than wood pellets under all conditions. This is due to their lower volatile matter content, which leads to reduced bubble formation during devolatilization, as well as their higher fixed carbon content, which increases the overall carbon available for conversion to CO_2. Increasing the superficial gas velocity from 0.15 to 0.3 m/s led to decreased CO_2 yields in packed configurations, due to shorter gas residence times and dilution effects. ECA packing exhibited material losses at 0.3 m/s, likely due to co-fluidization and attrition. Overall, RMSR packing demonstrated superior and more stable performance across all tested conditions.

Keywords: Chemical Looping Combustion, Packed-Fluidized Bed Reactor, Biomass, Ilmenite, CO_2 yield, Carbon capture.

Acknowledgements

I would like to express my sincere gratitude to my supervisor, Nasrin Nemati, and my examiner, Magnus Ryndén, for their invaluable guidance and support throughout this thesis project. Their expertise, constructive feedback, and continuous willingness to help have been essential to the completion of this work.

I would also like to sincerely thank the research engineers at the M7 Laboratory, Johannes Ohlin, Jessica Malene Bohwalli, and Rustan Hvitt. They generously shared their knowledge and contributed greatly to creating a productive, supportive, and enjoyable working environment.

My deepest thanks go to my family for their constant love, encouragement, and support. Their belief in me has been a source of strength and motivation throughout my studies.

Finally, I would like to acknowledge all those individuals around the world who strive to bring kindness, knowledge, compassion, and hope to others. In particular, I would like to honor the people of my home country, Iran, whose resilience and pursuit of a brighter future during these challenging times are source of inspiration to me. It is the efforts of such individuals that give meaning and purpose to our shared human experience.

گل بی خار میسر نشود در بستان/ گل بی خار جهان مردم نیکوسیرند

سعدیا مرد نکونام نمیرد هرگز/ مرده آن است که نامش به نکویی نبرند

Saeid Davam, Gothenburg, June 2026

سعید دوام، گوتنبرگ، خرداد ماه ۱۴۰۵

Table of Contents

List of Figures

List of Tables

Acronyms

NZE	Net Zero Emission
CCUS	Carbon Capture Utilization and storage
BECCS	Bioenergy with Carbon Capture and Storage
DACCS	Direct Air Carbon Capture and Storage
FBR	Fluidized Bed Reactor
PFBR	Packed-Fluidized Bed Reactor
RMSR	Random Metal Saddle Ring
ECA	Expanded Clay Aggregate
MP	Measurement Point
TP	Temperature and Pressure

Nomenclatures

Constant		
g	Gravitational force	*9.82 m.s^{-2}*
R	Universal gas constant	*8.314 j mol^{-1}.k^{-1}*
Variable		
ρ_f	Fluid density	*kg.m^{-3}*
ρ_p	Solid particle density	*kg.m^{-3}*
ε_{mf}	Voidage at minimum fluidization velocity	-
ε	Voidage	-
Δp_{bed}	Pressure drops across the bed	*kPa*
μ	Viscosity of fluid	*N.s.m^{-2} or Pa.s*
d_p	Particle size	*μm*
$\overline{dp}$	Average particle size distribution	*μm*
U	Superficial fluidization velocity	*m.s^{-1}*
U_{mf}	Minimum fluidization velocity	*m.s^{-1}*
H	Bed height	*m*
T	Temperature	*K or $^{\circ}$C*
$\dot{V}_i$	Volumetric flow rate of species i	*m^3.s^{-1}*
$\dot{m}_i$	Mass flow rate of species i	*kg.s^{-1}*
m_i	Mass of species i	*kg*
M_i	Molar mass of species i	*kg.mol^{-1}*
x_i	Mass fraction of ilmenite on each sieve	-
m_{sample}	Mass of ilmenite	*kg*
m_{void}	Mass of the added water	*kg*
m_{tot}	Total mass of water	*kg*
Other symbols		
Re_{mf}	Reynolds number at minimum fluidization	-
Ar	Archimedes number	-

1 Introduction

Human activities have increased significantly in recent decades, with fossil fuel combustion, deforestation, and industrial processes acting as major contributors to the acceleration of global warming and climate change.[1] Atmospheric CO_2 concentration has risen from approximately 280 ppm in the pre-industrial period to around 400 ppm today, corresponding to an estimated increase of about 0.8 °C in global mean temperature.[2] The 2024 Global Carbon Budget reports that global fossil CO_2 emissions rose to a record 37.4 Gt in 2024, corresponding to an increase of about 0.8% relative to 2023.[3] A major consequence of this trend is the increasing frequency of extreme weather events, including droughts, floods, wildfires, and hurricanes, as well as accelerated glacier melting, which contributes to rising sea levels.[2]

To address these challenges, numerous international Conferences of the Parties have been held under the UNFCCC framework, with the Paris Agreement in 2015 being the most significant milestone. In this agreement, 197 parties aimed to keep global warming well below 2 °C above pre-industrial levels, while also pursuing efforts to limit the temperature increase to 1.5 °C.[1]

The International Energy Agency has developed a Net Zero Emissions (NZE) scenario aiming to achieve global carbon neutrality by 2050. This pathway outlines several key pillars for decarbonizing the global energy system, including improvements in energy efficiency, changes in human behavior, large-scale electrification, expansion of renewable energy sources, deployment of hydrogen and hydrogen-based fuels, increased use of bioenergy, and implementation of carbon capture, utilization, and storage (CCUS). [4]

CCUS plays an important role in achieving net-zero CO_2 emissions by mitigating emissions from existing industrial facilities, providing solutions for sectors that are difficult to decarbonize, and enabling carbon dioxide removal from the atmosphere through approaches such as bioenergy with carbon capture and storage (BECCS) and direct air carbon capture and storage (DACCS).[4] Among the available carbon capture technologies, Chemical Looping Combustion (CLC) is considered a promising approach due to its inherent CO_2 separation capability, which eliminates the need for energy-intensive gas separation processes. Therefore, the overall energy penalty associated with carbon capture significantly reduces.[5]

The CLC system is normally composed of two interconnected Fluidized Bed Reactor (FBR): an air reactor and a fuel reactor as shown in Figure 1.1. Oxygen carrier in the form of metal oxide particles transfer oxygen between the two reactors. Thus, the Nitrogen is prevented from entering the fuel reactor. Fuel reacts with the oxygen carrier in the fuel reactor and forms CO_2 and H_2O, and after condensation of H_2O, the flow coming from the fuel reactor will consist of almost pure CO_2. [6]

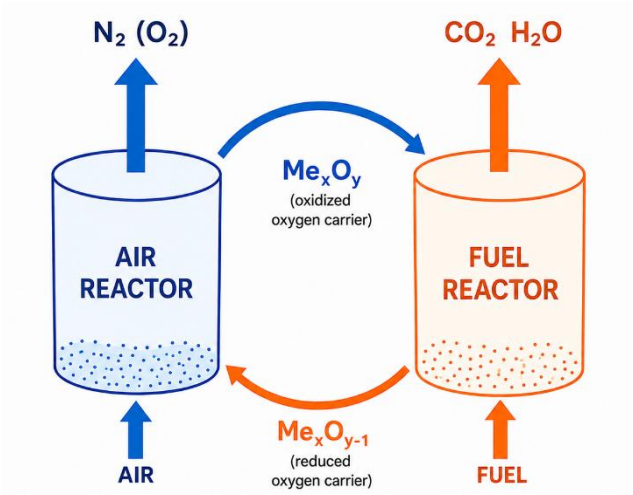

Figure 1.1.Simplified schematic of CLC

As mentioned, fluidized bed reactors are commonly used in CLC due to their excellent gas–solid mixing characteristics and their ability to facilitate the continuous transfer of solids between the two reactors. However, a key limitation of these systems is that once the superficial gas velocity exceeds the minimum fluidization velocity, excess gas is transported through the bed in the form of bubbles. These bubbles progressively grow through coalescence as they rise, increasing the bubble size and reducing the effectiveness of gas–solid mass transfer between the bubble and emulsion phases.[7] Consequently, gas–solid mass transfer can become limited, which negatively affects reactor performance. In CLC systems, where fuel conversion relies on gas–solid reactions between fuel species and oxygen carrier particles, poor contact between the phases can lead to lower conversion efficiency.[8] In biomass-fueled systems, this challenge becomes more pronounced because devolatilization releases gaseous species that generate bubbles within the bed, thereby affecting reactor hydrodynamics and gas–solid interactions.[9] To address this issue, packed or structured packings are introduced into the system to enhance gas–solid contact and improve mass transfer efficiency. [10] As shown in the Figure 1.2, the differences between a conventional fluidized bed reactor and a Packed-Fluidized Bed Reactor (PFBR) are illustrated.

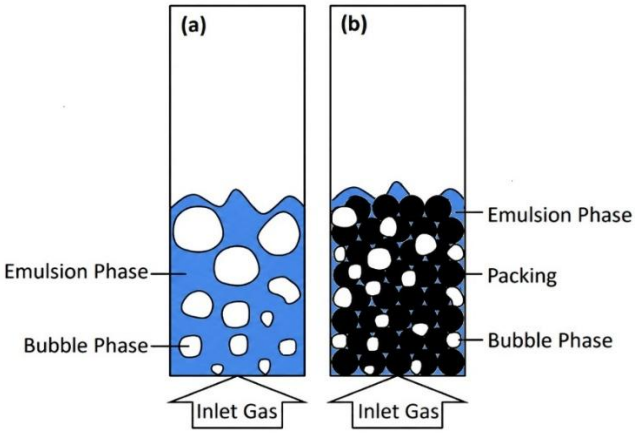

Figure 1.2. Schematics of FBR and PFBR

1.1 Aim

The aim of this project is to investigate biomass conversion in a Chemical Looping Combustion (CLC) process within Packed Fluidized Bed Reactor (PFBR). This study evaluates the effects of two different packing materials, RMSR (random metal-thread saddle ring) and expanded clay aggregate (ECA), and two different superficial velocities ,0.15 and 0.3 m/s, on the conversion yield of two types of fuel including wood pellets and torrefied wood pellets.

1.2 Limitation

Several limitations are associated with this study. First, gas analysis was conducted at a single outlet measurement point located 79.65 cm above the distributor plate. Consequently, gas composition along the reactor height could not be assessed, limiting the understanding of reaction progress and gas conversion within different regions of the bed. In addition, small variations in the biomass feed mass were observed between runs (3.27–3.33 g), which may have contributed to minor differences in the calculated yields. Furthermore, significant losses of ECA packing material were observed during experiments conducted at a superficial velocity of 0.3 m/s. These losses were likely caused by co-fluidization and particle attrition, which may have affected the reliability of the results obtained for the ECA configuration at higher velocities, particularly after multiple experimental repetitions. The measurement of H_2 was challenging due to its low concentration levels, particularly in experiments involving packing materials, which may have increased the uncertainty in the measured gas composition. Finally, all experiments were conducted at a fixed temperature of 900 °C and a single bed height; therefore, the influence of these parameters on packing performance and fuel conversion was not investigated.

2 Theory

2.1 Fluidization

When fluid passes through a packed bed at low velocity, the particles remain stationary and the fluid flows through the void spaces between them. In this regime, known as the fixed bed regime, the drag force applied by the fluid on the particles is smaller than the gravitational force acting on the solids ($U < U_{mf}$).

As the fluid velocity increases, a point is reached where the drag force becomes equal to the gravitational force. The corresponding velocity is called the minimum fluidization velocity (U_{mf}). At this point, the particles become suspended and the bed starts to fluidize.

In liquid–solid fluidized beds, increasing the velocity beyond U_{mf} generally results in a smooth and progressive expansion of the bed. However, gas–solid fluidized beds behave differently. When the gas velocity exceeds the minimum fluidization velocity, instabilities such as bubble formation and gas channeling occur[7], as shown in the Figure 2.1.1.

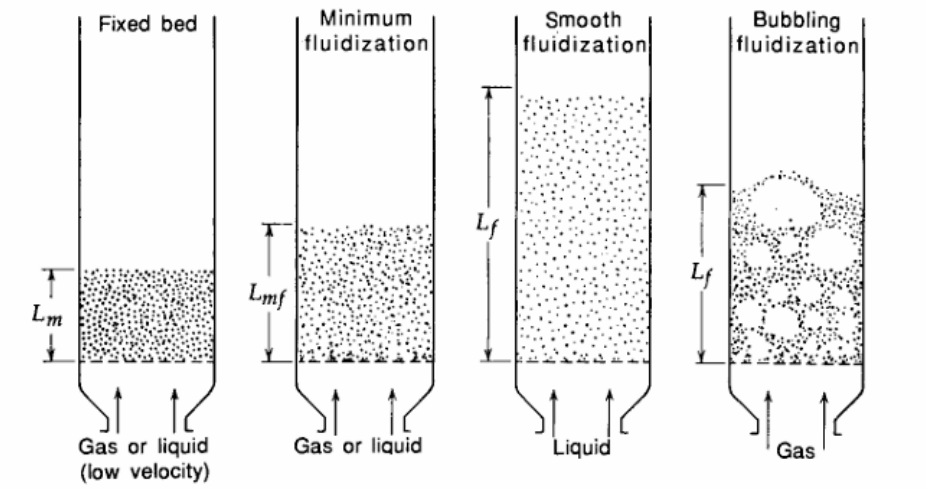

Figure 2.1. Different types of solid–fluid contact in batch systems.

According to Geldart [7], the behavior of a fluidized bed depends on the particle size distribution. In gas–solid systems, fluidization characteristics are classified into four Geldart groups based on the density difference between the fluidizing gas and the solid particles, as well as the particle size. The solid particle used in this project belongs to Geldart group B. Group B particles are generally sand-like materials with particle sizes in the range of approximately $40\,\mu m < d_p < 500\,\mu m$and particle densities between 1.4 and $4\,g/cm^3$, as shown in Figure2.2. These particles typically exhibit bubbling fluidization behavior once the minimum fluidization velocity is exceeded. Small bubbles initially form at the gas distributor and gradually grow and coalesce as they rise through the bed. The bubble size increases approximately linearly with both the height above the distributor and the excess gas velocity $(U-U_{mf})$.

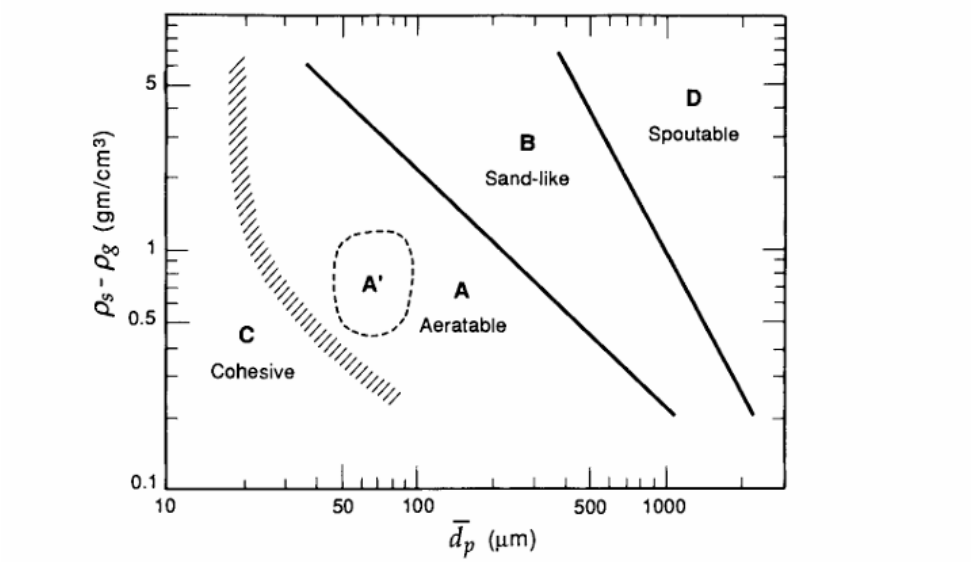

Figure 2.2. Geldart classification of solids

2.2 U_{mf} calculation

The motion of fluidization is described by a dimensionless number called the Archimedes number (Ar). In other words, the Archimedes number represents the relation between gravitational forces and viscous forces acting on a particle in a fluid. The Archimedes number is defined as:

$$Ar = \frac{{d_p}^3 \rho_f (\rho_p - \rho_f) g}{\mu^2} \qquad 2\text{-}1$$

The Reynolds number at minimum fluidization is expressed in terms of the minimum fluidization velocity $U_{mf}(m/s)$ as:

$$Re_{mf} = \frac{U_{mf} d_p \rho_p}{\mu} \qquad 2\text{-}2$$

For coarse particles, the relationship between the Reynolds number at minimum fluidization and the Archimedes number is given by the empirical correlation:[11]

$$Re_{mf} = (\,(28.7^2) + 0.0494\, Ar)^{1/2} - 28.7) \qquad 2\text{-}3$$

2.3 Pressure drops in fluidized bed

Passing fluid through a packed bed of particles results in a pressure drop across the bed. As the superficial velocity increases, the pressure drop also increases until a point is reached where the apparent weight of the particles is equal to the drag force exerted by the fluid $\left(U = U_{mf} \right)$. At this condition, the pressure drop reaches its maximum value (Point A), corresponding to the onset of fluidization.

Beyond this point, at higher velocities (Points B and C), the system operates in the fluidized bed regime, where the pressure drop remains approximately constant despite further increases in velocity.

For the calculation of pressure drop in the fluidized regime (B–C region), the pressure drop can be assumed to be equal to the weight of the solids per unit cross-sectional area of the bed:

$$\Delta p_{bed} = H\left(1 - \varepsilon_{mf}\right)(\rho_p - \rho_f)g \qquad 2\text{-}4$$

where $\varepsilon_{mf}(-)$ is the void fraction at minimum fluidization, $H(m)$ is the bed height, $\rho_p(kg/m^3)$ is the particle density, and $\rho_f(kg/m^3)$ is the fluid density. Figure 2.3, illustrates the variation of pressure drop and superficial velocity.[11]

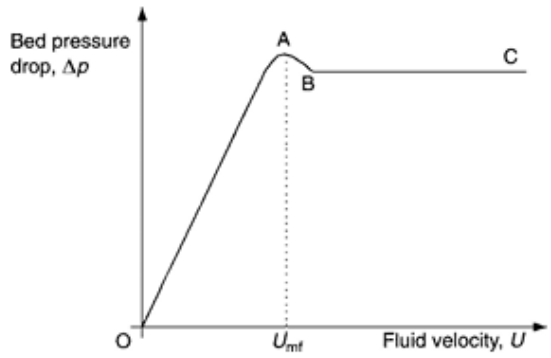

Figure 2.3.Pressure Drop as a Function of Fluid Velocity in a Fluidized Bed

2.4 Reactions

During biomass oxidation, the first stage is drying, during which the biomass loses its moisture content. This is followed by pyrolysis, where volatile compounds are released and char is formed as a solid residue. Pyrolysis generates various products; however, products are simplified to only CH_4. CO, and H_2. It should be noted that higher hydrocarbons are also formed, but in much smaller quantities. These species have a minor impact on the overall mass and energy balance. Due to the limited contact between the oxygen carrier and the char, gasification is required. the char can react with steam or CO_2 to produce additional combustible gases. These volatile then are oxidized through reactions with the oxygen carrier. The reactions occurring in the reactor are summarized below.[12]

Drying:

$$biomass\ (s) \rightarrow dry\ biomass(s) + H_2O\ (g) \quad 2\text{-}5$$

Pyrolysis:

$$dry\ biomass\ (s) \rightarrow C\ (char)(s) + volatile\ matters\ (CO, CH_4\ and\ H_2)\ (g) \quad 2\text{-}6$$

Gasification:

$$C\ (char)\ (s) + H_2O\ (g) \rightarrow CO\ (g) + H_2\ (g) \quad 2\text{-}7$$

$$C\ (char)\ (s) + CO_2\ (g) \rightarrow 2CO\ (g) \quad 2\text{-}8$$

Oxidation:Type equation here.

$$4M_xO_y\ (s) + CH_4\ (g) \rightarrow 4M_xO_{y-1}\ (s) + CO_2\ (g) + 2H_2O\ (g) \quad 2\text{-}9$$

$$M_xO_y\ (s) + CH_4\ (g) \rightarrow M_xO_{y-1}\ (s) + CO\ (g) + 2H_2\ (g) \quad 2\text{-}10$$

$$M_xO_y\ (s) + H_2\ (g) \rightarrow M_xO_{y-1}\ (s) + H_2O\ (g) \quad 2\text{-}11$$

$$M_xO_y\ (s) + CO\ (g) \rightarrow M_xO_{y-1}\ (s) + CO_2\ (g) \quad 2\text{-}12$$

Water-gas shift

$$CO\ (g) + H_2O\ (g) \leftrightarrow CO_2\ (g) + H_2\ (g) \quad 2\text{-}13$$

2.5 CLC fuel conversion yield

To be able to compare the fuel conversion yield for each experiment, mass balance on carbon is made. g of C as CO2 release per mass of carbon in biomass in´s calculated. Where mass of carbon in biomass is based on the reactions is the amount of carbon in CO CO2 CH4.

$$Y_{CO_2} = \frac{m_{C,CO_2}}{m_{C,biomass}} = \frac{m_{C,CO_2}}{m_{C,CH_4} + m_{C,CO} + m_{C,H_2}} \quad 2\text{-}14$$

The carbon mass in each gaseous species was calculated based on the measured volumetric gas concentrations recorded throughout the combustion process. Since nitrogen is assumed to behave as an inert gas, its molar flow rate is considered constant between the inlet and outlet streams. Therefore, a nitrogen balance can be applied to determine the total outlet gas flow rate:

$$x_{N_2,in}\dot{V}_{in} = x_{N_2,out}\dot{V}_{out} \quad 2\text{-}15$$

The outlet nitrogen concentration was determined from the measured outlet gas composition according to:

$$x_{N_2,out} = 1 - (x_{CO_2,out} + x_{CO,out} + x_{CH_4,out} + x_{H_2,out}) \quad 2\text{-}16$$

Using the calculated outlet volumetric flow rate, the volumetric flow rate of each gaseous component ($i = CO_2, CO, and\ CH_4$)was determined according to:

$$x_{i_{out}} \dot{V}_{out} = \dot{V}_{i,out} \quad \textit{2-17}$$

The mass flow rate of each species was then calculated using the ideal gas law:

$$\dot{m}_{i,out} = \frac{P\dot{V}_{i,out}\, M_i}{RT} \quad \textit{2-18}$$

Finally, the total mass of each gaseous species produced during combustion was obtained by integrating the mass flow rate over the combustion period:

$$m_{i,out\ total} = \sum_{t=start}^{t=end} \dot{m}_{i,out} \quad \textit{2-19}$$

3 Methodology

The material preparation in this work is carried out in laboratory M3 and the experimental work is conducted in laboratory M7 at Chalmers University of Technology. The reactor used in this study is called Reactor X.

3.1 Reactor

The experiments are carried out in a laboratory-scale high-temperature reactor constructed of 253 MA steel with a height of 1.27 m and inner diameter of 7.8 cm. The reactor is positioned inside an electrical furnace capable of heating it up to 1000 °C. The reactor set up is shown in Figure 3.1. The top of reactor is open and located within a metal fume hood to ensure effective exhaust gas ventilation.

Figure 3.1: Reactor X inside the furnace

The reactor is equipped with a wind box, at top of which a gas distributor plate is installed. The plate contains 61 orifices, each with a diameter of 0.6 mm. Gases and vapor, including steam, air, and nitrogen, are introduced through these orifices. The reactor has total of 16 measurement tube connections: 8 located on the front side and 8 on the back side of reactor wall. The rear connections are used for thermocouples and pressure sensors. The front connections are used for gas sampling. The axial positions of these connections measured relative to the gas distributor plate, are provided in Table 3-1.

Table 3-1: The position of measurement points (MPs) from the gas distributor plate

Measurement Points	Measured data	Height (cm)
8	Temperature, pressure, and gas concentration	79.65
7	Temperature, pressure, and gas concentration	63.65
6	Temperature, pressure, and gas concentration	47.65
5	Temperature, pressure, and gas concentration	31.65
4	Temperature, pressure, and gas concentration	15.65
3	Temperature, pressure, and gas concentration	13.65
2	Temperature, pressure, and gas concentration	8.88
1	Temperature, pressure, and gas concentration	3.65
Windbox	Temperature and pressure	- 4.00

In this study, a gas sampling pipe is connected to the reactor at point 8. This point is located 79.65 cm above the distributor plate. The pipe is linked to an online gas analyzer, the SICK GMS810 gas analyzer, positioned adjacent to the reactor, as it is shown in Figure 3.2. The analyzer measures the volumetric concentrations of H_2, CH_4, O_2, CO_2, and CO. The sampled gas flows through a PTFE (Polytetrafluoroethylene) tube heated to 180 °C. This prevents condensation. The gas then passes through a conditioning unit, where steam is removed as liquid water. Finally, the dry gas stream is directed to the analyzer. The analyzer is connected to a computer, allowing real-time monitoring of the results using software called LabVIEW. Additionally, the gas flow into the reactor is controlled through the same software.
To enable the introduction of solid biomass directly into the reactor bed rather than onto the bed surface, a feeding system was designed and integrated into the reactor. The feeding system consists of a 253 MA steel pipe with an inner diameter of 15.73 mm and a length of 1 m. The lower end of the feeding pipe is positioned inside the bed, and its height relative to the reactor distributor plate can be adjusted manually. In all experiments conducted in this work, the pipe outlet was fixed at approximately 24 cm above the distributor plate. The top of the feeding system is equipped with a funnel for biomass loading. Two manually operated ball valves are installed below the funnel. Between these valves, a horizontal pipe connected to an N_2 gas cylinder and rotameter supplies approximately 1 NL/min of nitrogen. A second horizontal pipe and rotameter are installed below the second valve, providing an additional N_2 flow of approximately 1 ln/min.
A continuous nitrogen flow is maintained through the lower injection line to ensure smooth downward transport of the biomass particles and to prevent the accumulation of volatiles inside the feeding pipe. During operation, the upper valve is initially opened, and nitrogen is introduced through the intermediate injection line to purge oxygen from the section between the two valves. The upper valve is then closed, and biomass is loaded into the funnel. After reopening the upper valve, the biomass falls into the intermediate section between the valves. The upper valve is subsequently closed again, and nitrogen is introduced to pressurize this section. Finally, the lower valve is opened, allowing the fuel to be transported into the reactor without blockage. This feeding configuration ensures that biomass is introduced directly into the dense bed region.

The schematic of the reactor, including the measurement points, feeding system, and nitrogen injection points, is shown in Figure 3.3.

Figure 3.2 : Reactor X inside the furnace with SICK gas analyzer

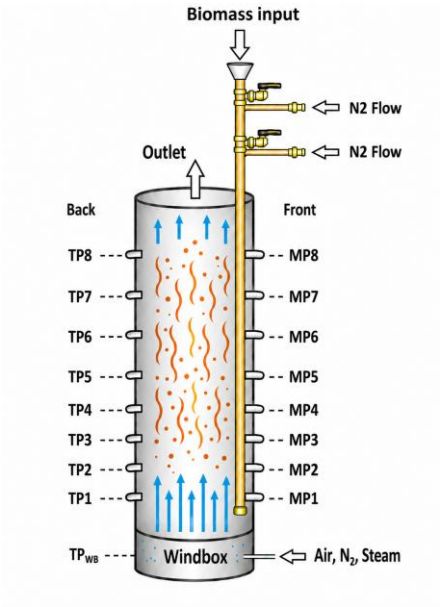

Figure 3.3: Reactor X schematic with Measurement Points (MPs) for TP (temperature, Pressure), and gas concentration, feeding system, and nitrogen injection pipes.

3.2 Material

The oxygen carrier bed material used for the chemical-looping combustion (CLC) experiments is ilmenite concentrate. The packings employed in the system are expanded clay aggregate (ECA) with an average diameter of 12 mm and 25 mm random metal-thread saddle ring (RMSR). The fuels investigated in this study are wood pellets and torrefied wood pellets. Further details regarding the oxygen carrier bed material, packings, and fuels are provided in the following sections.

3.2.1 Oxygen Carrier

Ilmenite concentrate, commonly referred to as ilmenite, is one of the most widely used oxygen carriers in solid fuel chemical looping combustion. It is primarily composed of iron–titanium oxide minerals. In simplified representations of chemical-looping systems, the reduced form is typically described as ilmenite ($FeTiO_3$), while the oxidized form is assumed to consist mainly of pseudobrookite (Fe_2TiO_5) and titanium dioxide (TiO_2). However, the actual reaction and phase compositions are more complex.[13]

The bulk density of ilmenite is determined using a density measurement apparatus shown in Figure 3.4. In this procedure, ilmenite is poured through the funnel into a cylindrical silver metal container with volume of 25 ± 0.03 cm^3. Once the container is filled, the surface is carefully leveled using a metal spatula to obtain an even surface. The filled container is then weighted. To improve the accuracy of the results, the measurement is repeated ten times, and the mean value is calculated. The resulting average bulk density is 1929.6 kg/m^3.

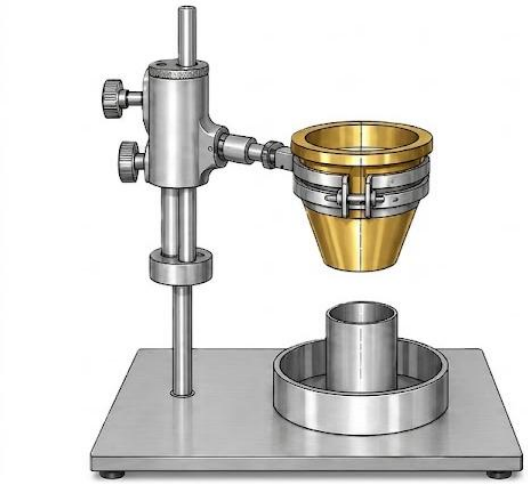

Figure 3.4 : Density measurement apparatus schematic

To determine particle size distribution of ilmenite, a 1000 g sample is used. The sample is sieved using a mechanical shaker (Figure 3.5) through a stack of sieves covering a size range of 45–425 µm for 15 minutes. After sieving, the ilmenite on each sieve is then collected and weighed separately. The results are presented in Table 3-2. Based on these mass fractions, the particle size distribution curve can be constructed as shown in Figure 3.6.

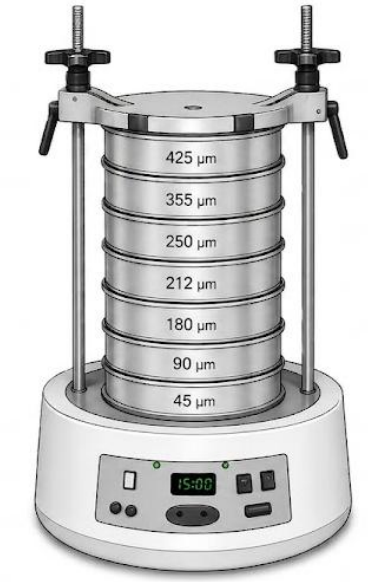

Figure 3.5: Mechanical shaker schematic

Table 3-2: Mass of ilmenite on each sieve

Sieve size (µm)	Mass of ilmenite (g)
425	0
355	3.5
250	360.7
212	198.7
180	145.7
90	287.7
45	3.6

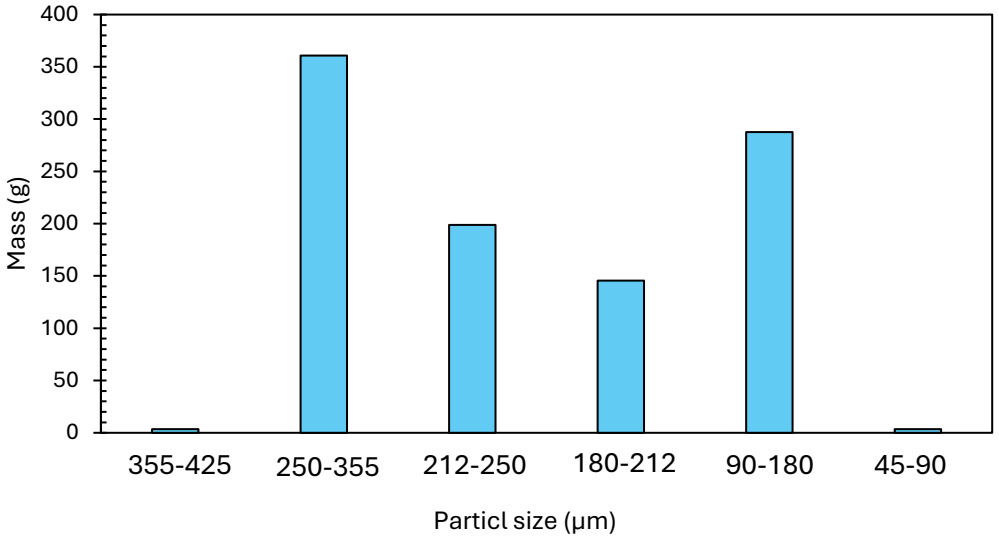

Figure 3.6: particle size distribution of ilmenite

The average particle size is calculated from the measured particle size distribution. Eq. 3-1 and Eq. 3-2 are applied. These are based on the mass retained on each sieve relative to the total sample mass. x_i (-) represents the mass fraction of ilmenite on each sieve, calculated as the mass retained on each sieve (m_i, kg) divided by the total sample mass (m_{sample}, kg). The average particle size $\overline{dp}$ is obtained from the inverse of the summation of x_i divided by the mean size between the corresponding sieve and the next larger sieve.[7]

$$x_i = \frac{m_i}{m_{sample}} \qquad 3\text{-}1$$

$$\overline{dp} = \frac{1}{\sum \frac{x_i}{dp_i}} \qquad 3\text{-}2$$

A summary of measured ilmenite bulk density, average particle size, and required mass for 40 cm unfluidized bed height are shown in Table 3-3:

Table 3-3: Ilmenite bulk density, average particle size, and required quantity

Bulk density (kg/m^3)	Average particle size (µm)	Required mass (kg)
1929.6	200.4	3.69

3.2.2 Packings

The packings used in this study are ECA and RMSR 25-3 shown in Figure 3.7 and Figure 3.8 respectively. ECA is a lightweight, porous ceramic material composed primarily of SiO_2, Al_2O_3, Fe_2O_3, CaO, and minor amounts of alkali oxides. Due to its porous structure, low density, thermal insulation properties, chemical stability, and fire resistance, ECA has been widely used in different applications including lightweight concrete, wastewater treatment systems, agricultural and horticultural applications, and drainage systems.[14]

The RMSR packing consists of stainless steel and is widely used as a packing material in chemical reactors due to its high void fraction and enhanced gas–liquid or liquid–liquid mass transfer characteristics. Their density and void fraction are determined prior to experiments.

Figure 3.7 : ECA packing

Figure 3.8: RMSR packing

To calculate void factor (ε, -) of packings, a container is first filled with water, and the total mass of the water (m_{tot}, kg) is noted. The container is then emptied and filled with the packing material. Water is added to fill the voids between the packing particles, and the mass of the added water (m_{void}, kg) is measured. The void factor is then calculated using Eq. 3-3 :

$$\varepsilon = \frac{m_{void}}{m_{tot}} \qquad 3\text{-}3$$

To determine the bulk density, a container of known volume and mass is filled with the packing material, and the mass difference is measured to obtain the mass of the packing. The bulk density is then calculated as the ratio of the packing mass to the container volume. Each measurement is repeated 10 times to improve accuracy and ensure reliability of the results.
To determine the required amount of packing, it is important to consider the properties of each material. RMSR, being metallic with a high void factor, can be used to fill the reactor bed up to a total height of 75 cm. in contrast, ECA packings consists of low-density spherical particles that tend to float and remain in the upper region of the bed during operation. Therefore, an ECA layer of approximately 25 cm is sufficient.
Table 3-4 presents the void factor, density, and required quantity of the packing materials.

Table 3-4: Packing void factor, density, and required quantity

Packings	Void Factor (-)	Density (kg/m^3)	Height (m)	Volume(m^3)	Required Mass (kg)
RSMR	0.96	192	0.75	0.0036	0.688
ECA	0.42	318.9	0.25	0.0012	0.381

3.2.3 Fuel

As previously mentioned, the fuels used in this study are wood pellets and torrefied wood pellets. These fuels are selected due to their differing volatile matter and fixed carbon contents, which enable investigation of their effects on the system performance.

The volatile and fixed carbon contents are determined using thermogravimetric analysis (TGA) TGA701 model manufactured by LECO. TGA measures the mass change of a sample as a function of temperature and time under a controlled atmosphere, typically N_2 or air, and allows quantification of moisture, volatile matter, fixed carbon, and ash content. The results of the TGA analysis for wood pellets and torrefied wood pellets are presented in Table 3-5.

Table 3-5: TGA results of wood pellet and torrefied wood pellets

	Wet basis (wt.%)				Dry basis (wt.%)		
Fuel	Moisture	Volatile	Ash	Fixed Carbon	Volatile	Ash	Fixed Carbon
Torrefied wood pellets	7.843	61.407	1.585	29.165	66.633	1.718	31.647
Wood pellets	7.028	75.237	0.692	17.040	80.927	0.743	18.328

3.3 Gases

Two superficial gas velocities are investigated: 0.15 m/s (Case A) and 0.3 m/s (Case B). The superficial gas velocity in a fluidized bed reactor is defined as the volumetric gas flow rate divided by the empty cross-sectional area of the reactor which represents the hypothetical gas velocity in the absence of solid particles.[7] The minimum fluidization velocity (U_{mf}), calculated using Equations 2.1–2.3, is 0.034 m/s. The lower gas velocity and higher gas velocity correspond to U/U_{mf} ratios of approximately 4.4 and 8.8, respectively. These values indicate that both cases operate within the bubbling fluidization regime. These conditions are achieved by adjusting the total gas flow rates during the oxidation and reduction steps to 10 and 20 NL/min, respectively.

The maximum capacity of the steam generator is approximately 12 NL/min. Therefore, during the fuel feeding (reduction) step, up to 10 NL/min of nitrogen is introduced to the reactor to ensure the desired superficial gas velocity is maintained. This also ensures a continuous minimum gas flow during gas switching from the reduction to the inert step.

It is important to note that the volumetric gas flow rates in NL/min were calculated based on the required superficial gas velocity and were subsequently converted to normal condition (0 °C and 1 atm). The corresponding gas flow rates and operating conditions for each step are summarized in Table 3-6.

Table 3-6: Gas flow rates of each step in NL/min for both A and B cases.

Step	Gas	Case A	Case B
Oxidation	Air	10 NL/min	20 NL/min
Inert	Nitrogen	10 NL/min	10 NL/min
Reduction	Nitrogen	5 NL/min	10 NL/min
	Steam	5 NL/min	10 NL/min

3.4 Experiment

In this study, two different fuels, two packing configurations, and two superficial gas velocities are investigated, resulting in a total of 12 experimental cases, as summarized in Table 3-7. It should also be noted that pressure, temperature, and gas analysis data are recorded at a sampling frequency of 1 Hz.

Table 3-7 : Test matrix

Number	Velocity(m/s)	Fuel	Packing
1	0.15	Wood pellet	-
2	0.15	Torrefied wood pellet	-
3	0.3	Wood Pellet	-
4	0.3	Torrefied wood pellet	-
5	0.15	Wood Pellet	RMSR
6	0.15	Torrefied wood pellet	RMSR
7	0.3	Wood Pellet	RMSR
8	0.3	Torrefied wood pellet	RMSR
9	0.15	Wood Pellet	ECA
10	0.15	Torrefied wood pellet	ECA
11	0.3	Wood Pellet	ECA
12	0.3	Torrefied wood pellet	ECA

3.4.1 Experimental procedure

For experiments involving packings, the packing material is first introduced into the reactor. Subsequently, the bed material is added while maintaining air flow to prevent particles from entering the windbox. Air flow of 5 NL/min is therefore established prior to bed material loading. After preparing the bed, the reactor is heated by setting the furnace temperature to 870 °C. Once stable conditions are reached, the temperature at thermocouple position TP1 stabilizes at 900 °C. In parallel, the auxiliary systems, including the steam generation unit, warm filter, and gas conditioning unit (comprising the condenser and suction pump) are switched on.
When all components reach stable operating conditions, the system is ready for the experimental runs. The detailed procedure for each experimental run is described:

1. Oxidation step: air is introduced into the reactor to oxidize the ilmenite oxygen carrier. Air flow rates of 20 NL/min and 10 NL/min are used for superficial gas velocities of 0.3 m/s and 0.15 m/s, respectively. This phase continues until the oxygen concentration measured by the SICK gas analyzer stabilized above 20.5%.
2. Inert step: Nitrogen is introduced at a flow rate of 10 NL/min to purge the reactor and remove the air from the system. This ensures that oxygen for combustion during the reduction step is provided solely by the ilmenite. The inert step is completed once the oxygen concentration stabilizes below 0.4%.
3. Reduction step: While maintaining the nitrogen flow according to Table 3.6, steam is introduced at flow rates of 8.04 g/s and 4.02 g/s for superficial gas velocities of 0.3 m/s and 0.15 m/s, respectively. Biomass is then fed into the reactor through the feeding system. In each experiment, six fuel pellets of similar size are introduced, with the intention of maintaining a constant total mass for all experimental runs. However, due

to minor weighing uncertainties, the total mass varies slightly between experiments, ranging from 3.27 to 3.33 g. After fuel addition, combustion begins and the oxygen carrier undergoes reduction. The reduction phase continues until the concentrations of combustion gases, particularly CO_2, decrease to near zero. At this point, the steam flow is stopped, and the reactor returns to the inert step.

After completion of the reduction step, the cycle is repeated starting from the oxidation step to regenerate the ilmenite oxygen carrier. Each operating condition is repeated 4–6 times to ensure reproducibility of the results.

3.4.2 Empty-bed experiments

To determine the pressure, drop across the bed material during the reduction phase, an empty-bed experiment is performed. The total pressure drop measured during each experimental run is obtained as the difference between the pressure in the windbox and at point 8 (Figure 3.3); and therefore, includes contributions from both the windbox and the bed material. To isolate the pressure drop across the bed, the windbox contribution must be determined separately. For this purpose, the reactor is operated without bed material under similar operating conditions as the reduction step. Nitrogen and steam are introduced at both superficial gas velocities, and the resulting pressure drop corresponds to the windbox contribution alone. By subtracting this value from the total pressure drop measured during the actual experiments, the pressure drop across the bed material can be determined.

4 Results and Discussion

As it was mentioned, chemical looping combustion (CLC) experiments are conducted using two solid fuels, wood pellets and torrefied wood, at two superficial fluidization velocities of 0.15 m/s and 0.3 m/s. Three bed configurations are investigated: no packing, RMSR packing, and ECA packing. At least four repeated experiments are performed for each operating condition to ensure reproducibility. For clarity and ease of comparison, one representative experimental run that best reflects the overall trend of repeated measurements was selected for each case and is presented in the following section. The complete set of repeated experiments is provided in Appendix A, while the selected representative runs are summarized in Table 4.1.

Table 4-1: Selected experimental runs as representatives

Fuel	Velocity (m/s)	No packing	RMSR	ECA
Wood pellet	0.15	3	3	5
	0.3	2	4	1
Torrefied wood pellet	0.15	1	2	4
	0.3	2	4	2

4.1 Gas concentration and pressure profiles

To evaluate the performance of the CLC process under different operating conditions, presented in Table 8, the profile of the CO_2, CH_4, CO, and H_2 over time are monitored for each experimental run. These concentration profiles are presented in Figures 4.1-4.4. Hydrogen is excluded from these comparative figures, as its concentration was very low and it is difficult to be measured accurately during operation. Therefore, it was assumed to be negligible in both RMSR and ECA configurations. However, in no packing configuration, the H_2 concentration is non-negligible. Therefore, the corresponding H_2 concentration profile for the no packing configuration is provided in the Appendix A.

(a)

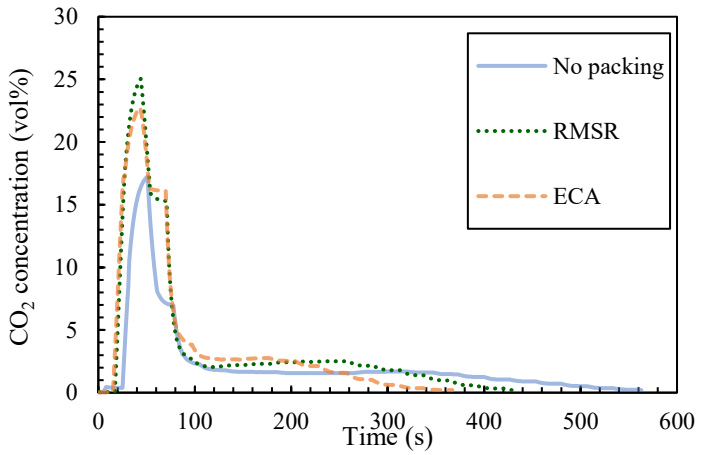

(b)

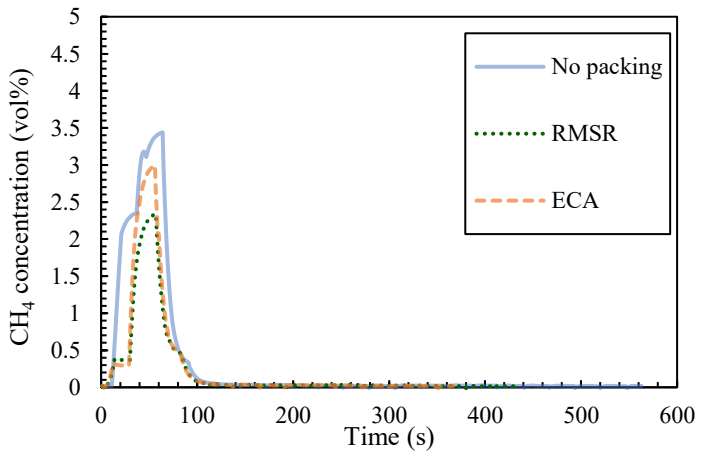

(c)

(d)

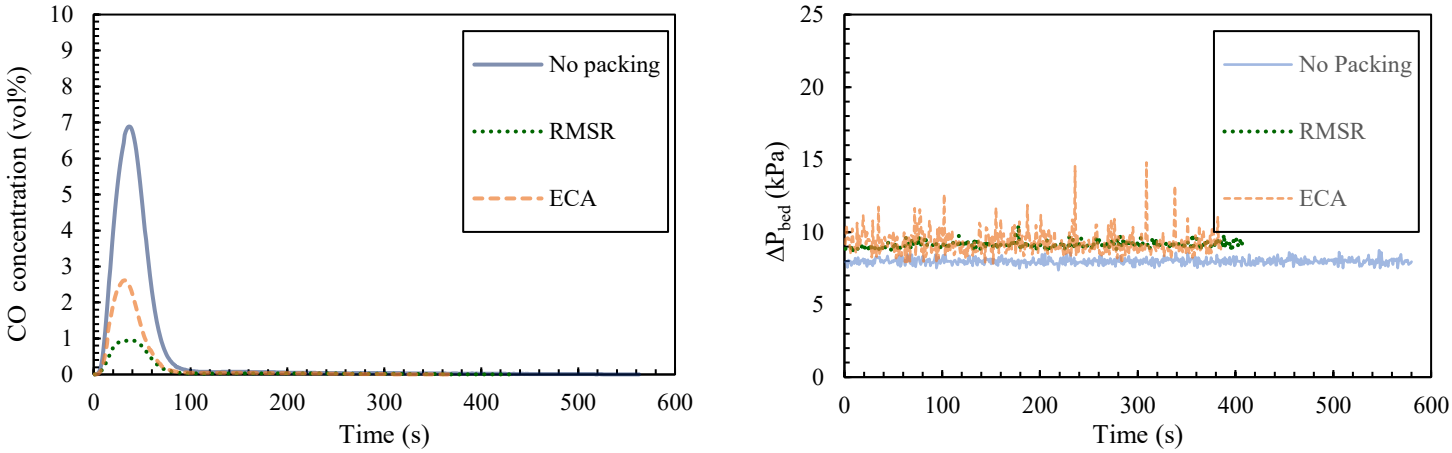

Figure 4.1. Outlet gas concentration and pressure profiles as a function of time for batch CLC experiments using wood pellet at a superficial gas velocity of 0.15 m/s and fuel reactor temperature of 900°C; comparing three bed configurations: No packing, RMSR, and ECA: (a) CO_2, (b) CH_4, (c) CO concentrations, and (d) bed pressure drop.

As shown in Figure 4.1a), the CO_2 profile exhibits a sharp initial peak followed by a prolonged tail. The peak corresponds primarily to rapid devolatilization and oxidation of released volatiles, while the tail reflects slower char conversion governed by steam gasification and subsequent oxidation of CO and H_2 by the oxygen carrier.[15] Figure 4.1 also shows that CO_2 concentrations increase when packings are introduced compared to the no-packing case. In contrast, CH_4 and CO concentrations decrease with packings. The maximum volumetric concentrations for wood pellet experiments at superficial gas velocities of 0.15 m/s under different reactor configurations are presented in the Table 4-2.

Table 4-2. Maximum concentration of CO2, CH4, and CO for wood pellet experiments at superficial gas velocities of 0.15m/s under no-packing, RMSR, and ECA bed configurations

	CO_2 peak (%)	CH_4 peak (%)	CO peak (%)
No Packing	17.2	3.4	6.9
RMSR	25.0	2.3	1.0
ECA	22.7	3.0	2.6

Relative percentage differences with respect to the no-packing case show that the CO_2 peak increases by 45% and 32% for RMSR and ECA, respectively, while CH_4 decreases by 32% and 13%, and CO decreases by 86% and 62%, respectively. Detailed information on volumetric gas fractions for each experimental run and repetition is provided in Table 7-1 and Table 7-2 in Appendix B.

As shown in Figure 4.1, RMSR packing enhances combustion efficiency compared to the no-packing case. The RMSR material has a high void fraction, Table 3-4, which allows the packings to distribute uniformly within the fluidized bed with only minor effects on the overall pressure drop (Figure 4.1(d)). The influence of RMSR packing on bubble dynamics has been previously investigated by Nemati et al.[10], in their study, experiments were performed using syngas and CO as gaseous fuels at 840°C for different bed heights. Their results showed that RMSR packing suppresses bubble formation and promotes the breakup of large bubbles into smaller ones. As bubble size decreases, the interfacial area between the bubble phase and the

emulsion phase increases. Consequently, gas–solid mass transfer is enhanced, improving contact between volatiles and the oxygen carrier. This leads to higher fuel conversion and increased CO_2 production compared to the bed without packing.

ECA packing also enhances combustion efficiency. Due to their lower density compared to the bed material, as presented in Table 3-4, ECA packings tend to accumulate in the upper region of the bed rather than staying at the bottom. A portion of the particles also becomes partially submerged at the bed surface. Similar to RMSR, this configuration can influence bubble dynamics by limiting the formation of large bubbles in the upper bed region. As bubbles rise, their interaction with the packed region promotes bubble disruption. In addition, we hypnotize that the accumulated ECA layer acts as a physical barrier that reduces the tendency of the light biomass particles to migrate to the bed surface. This helps retain the fuel within the dense bed region, improving contact between the released volatiles and the oxygen carrier. As a result, gas–solid interaction is enhanced, leading to improved conversion efficiency.

Moreover, in a previous study by Aronsson et al., blank experiment was conducted at an operating temperature of 915 °C using only sand and ECA packing, without the presence of oxygen carriers. In these experiments, syngas was used as fuel with a flow rate of 3 NL/min combined with 10 NL/min of inert gas. The results showed that ECA packing could absorb and carry oxygen. Therefore, they concluded that ECA packing not only enhances CO_2 conversion by modifying the hydrodynamics of the bed through improved gas–solid contact but may also contribute directly to oxidation by acting as an additional oxygen carrier.[13]

In Figure 4.2, the outlet gas concentration profiles for wood pellet combustion are presented for the higher superficial gas velocity of 0.3 m/s.

(a)

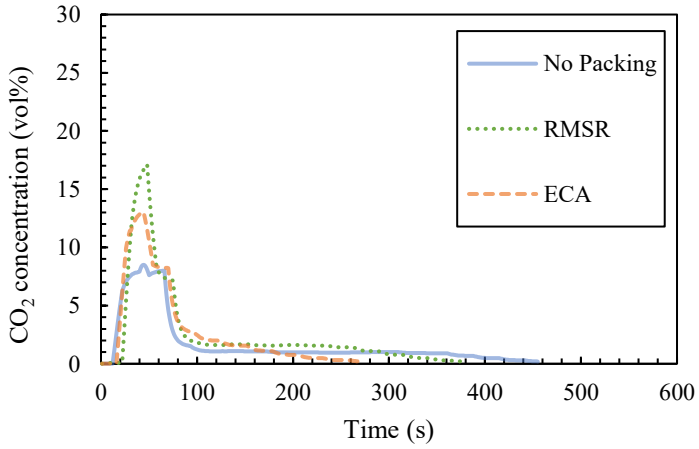

(b)

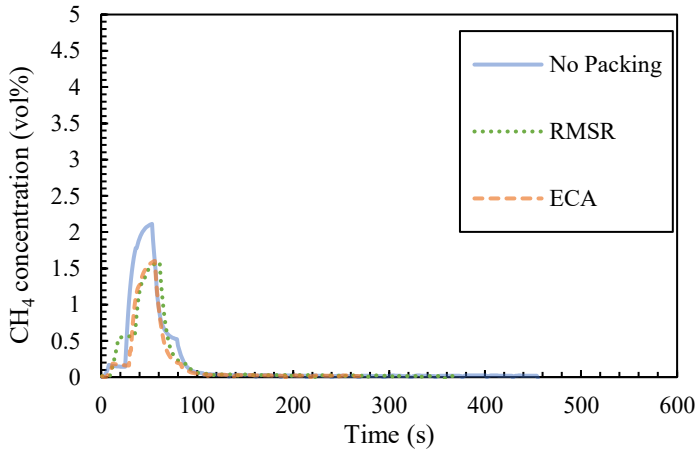

(c)

(d)

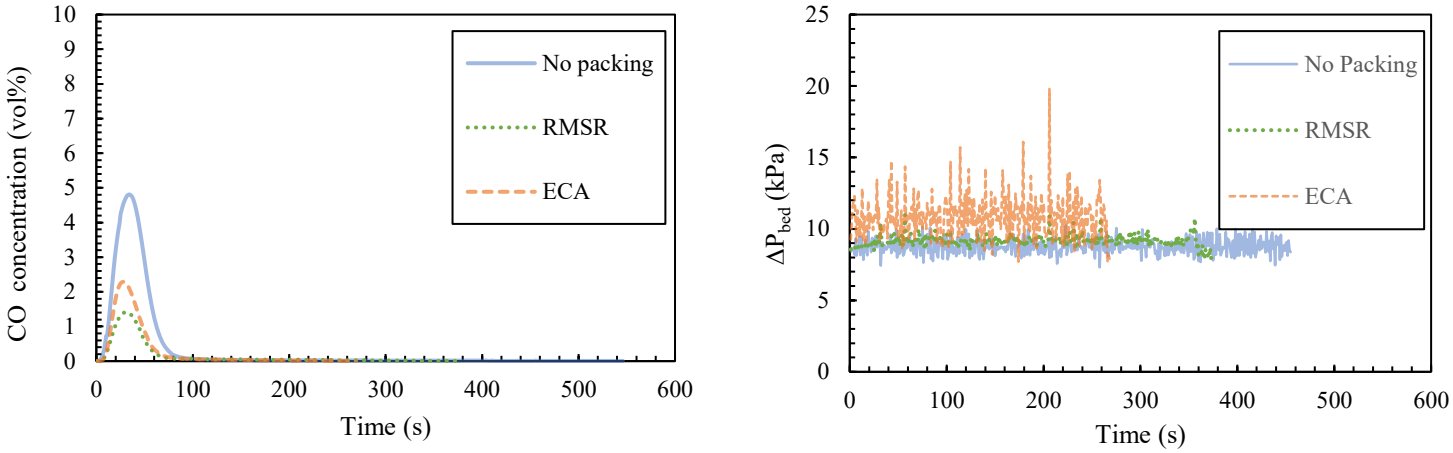

Figure 4.2. Outlet gas concentration and pressure profiles as a function of time for batch CLC experiments using wood pellet at a superficial gas velocity of 0.3 m/s and fuel reactor temperature of 900°C; comparing three bed configurations: No packing, RMSR, and ECA: (a) CO_2, (b) CH_4, (c) CO concentrations, and (d) bed pressure drop.

Figure 4.2 presents the same fuel and reactor temperature conditions as Figure 4.1, but at a higher superficial gas velocity of 0.3 m/s. This enables a direct comparison of the effect of increasing superficial gas velocity on reactor performance in both packed and unpacked fluidized beds. As can be seen in Figure 4.2, The maximum volumetric concentrations for wood pellet experiments at superficial gas velocities of 0.3 under different reactor configurations are presented in the Table 4-3.

Table 4-3. Maximum concentration of CO2, CH4, and CO for wood pellet experiments at superficial gas velocities of 0.3m/s under no-packing, RMSR, and ECA bed configurations

	CO_2 peak (%)	CH_4 peak (%)	CO peak (%)
No Packing	8.5	2.1	4.1
RMSR	17.1	1.6	1.4
ECA	13.1	1.6	2.3

Relative percentage differences with respect to the no-packing case show that the CO_2 peak increases by 102% and 54% for RMSR and ECA, respectively, while CH_4 decreases by 33% and 24%, and CO decreases by 65% and 44%, respectively.

As discussed in the theory section, superficial gas velocity influences both gas residence time and bubble size. At higher velocities, the gas passes through the bed more rapidly, which reduces the residence time and decreases the gas–solid contact. In addition, an increase in superficial velocity generally leads to the formation of larger bubbles.[7] These larger bubbles reduce the interfacial area between the bubble phase and the emulsion phase, thereby decreasing mass transfer between the two phases. Furthermore, increasing the fluidization velocity introduces a dilution effect. A higher gas flow rate corresponds to increased steam and inert gas flow, while the biomass feeding rate remains constant. As a result, the partial pressure of volatile species released from the biomass is reduced. Since reaction rates are generally dependent on reactant partial pressures, this leads to lower reaction rates and reduced CO_2 formation. In a previous study on dilution effects, Sadjadi et al. investigated the methane conversion, under

diluted conditions using N_2. Their results showed that increasing dilution negatively affects methane conversion.[16]

Figure 4.3 presents the outlet gas concentration profiles for batch CLC of torrefied wood pellets at a superficial gas velocity of 0.15 m/s.

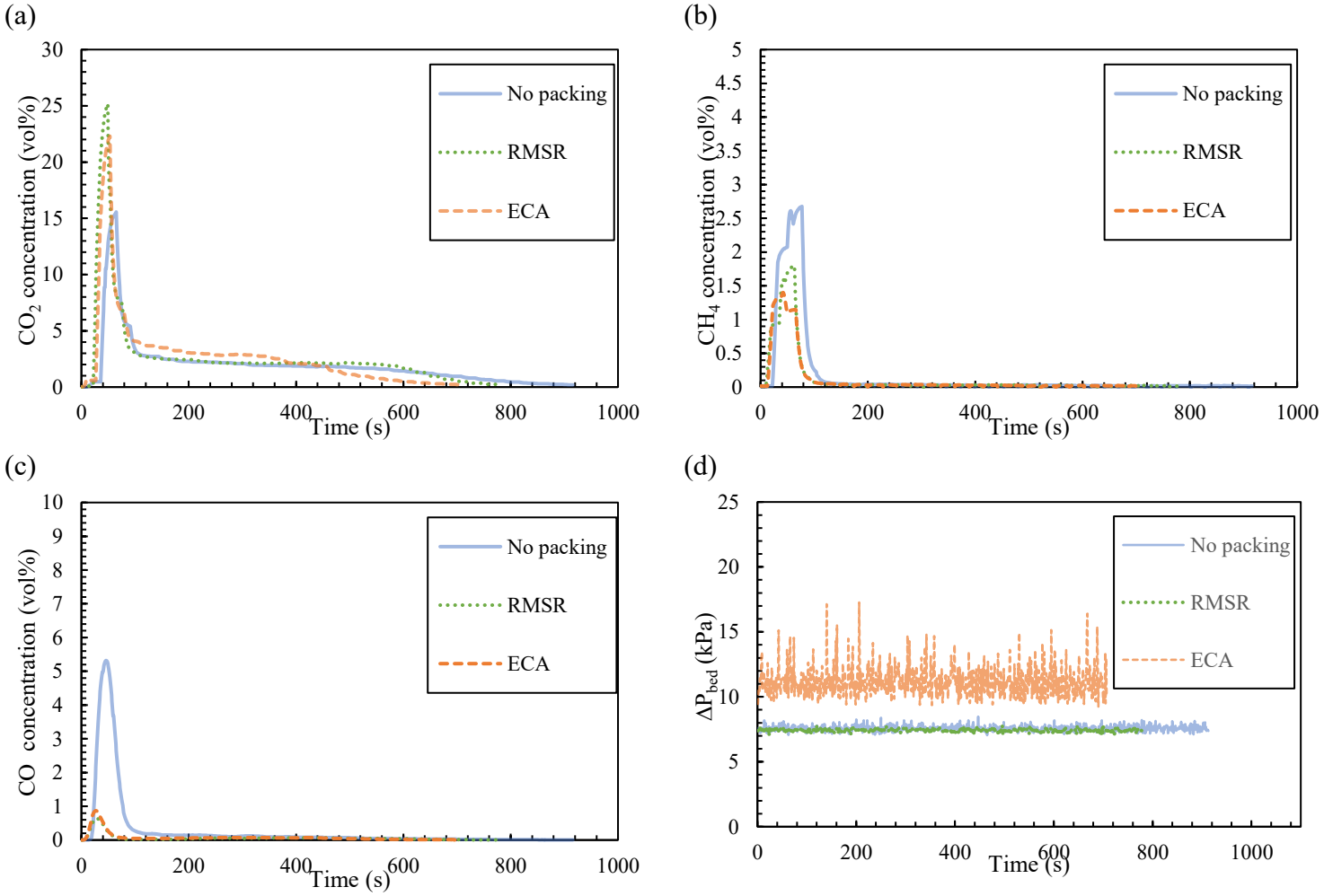

Figure 4.3. Outlet gas concentration and pressure profiles as a function of time for batch CLC experiments using torrefied wood pellet at a superficial gas velocity of 0.15 m/s and fuel reactor temperature of 900°C; comparing three bed configurations: No packing, RMSR, and ECA: (a) CO_2, (b) CH_4, (c) CO concentrations, and (d) bed pressure drop.

Figure 4.3 presents a similar superficial gas velocity and reactor temperature conditions as Figure 4.1, but with torrefied wood pellet as the second fuel with different characteristics. This enables a comparison of the effect of fuel on reactor performance in both packed and unpacked fluidized beds. To enable a more meaningful comparison, the total volumetric concentration of each outlet gas (excluding N_2, H_2) was calculated using Equations 2-15–2-17. The results are presented in the Table 4-4.

Table 4-4. Total volumetric concentration of outlet gases (Excluding N_2 and H_2) for wood pellet and torrefied wood pellet experiments at superficial gas velocity of 0.15m/s under no-packing, RMSR, and ECA bed configurations

Fuel	Packing	CO_2 (%)	CH_4 (%)	CO (%)
Wood Pellet	No Packing	76.8	8.1	15.1
	RMSR	92.1	5.2	2.9
	ECA	88.1	6.2	5.7
Torrefied Wood Pellet	No Packing	81.3	7.0	11.7
	RMSR	93.6	4.3	2.1
	ECA	93.3	4.1	2.7

Relative percentage differences with respect to the wood pellets case show that the total CO_2 volumetric concentration for torrefied wood pellet increases by 6 %, 2 %, and 6 % for no packing, RMSR, and ECA, respectively while total CH_4 volumetric concentration decreases by 14 %, 17 %, and 34 % and total CO volumetric concentration decreases by 22 %, 28 %, and 53 % , respectively.

This comparison shows that torrefied wood pellet produces higher CO_2 concentration compared to wood pellets, which is related to differences in volatile matter and fixed carbon content. As shown in Table 3-5, wood pellets contain a higher volatile matter fraction, resulting in a more rapid release of gaseous species during devolatilization. As shown in Figure 4.14.1 and Figure 4.34.3, the initial peak region is dominated by rapid devolatilization, where the volatile release rate is significantly higher than the subsequent char gasification rate. A high volatile release rate can locally increase gas generation within the bed, potentially promoting larger bubble formation and reducing gas–solid contact efficiency. In contrast, torrefied wood pellet releases less volatiles due to its lower volatile content, which may contribute to smaller bubbles and thus improved gas–solid interaction and higher CO_2 conversion.

In addition, torrefied wood pellet exhibits longer combustion times than wood pellets across all reactor configurations. As can be seen by comparing Figure 4.14.1 and Figure 4.34.3, the combustion time increases from 564 s to 917 s for no packing configuration, 423 s to 779 s for RMSR, and 368 s to 708 s for ECA. This behavior is mainly due to higher fixed carbon content of torrefied wood pellet. After devolatilization, the remaining char is converted through gasification reactions, which are considerably slower than volatile conversion. Consequently, fuels with higher char content are expected to exhibit longer overall conversion times.

In Figure 4.4, the outlet gas concentration profiles for torrefied wood pellet combustion are presented for the higher superficial gas velocity of 0.3 m/s.

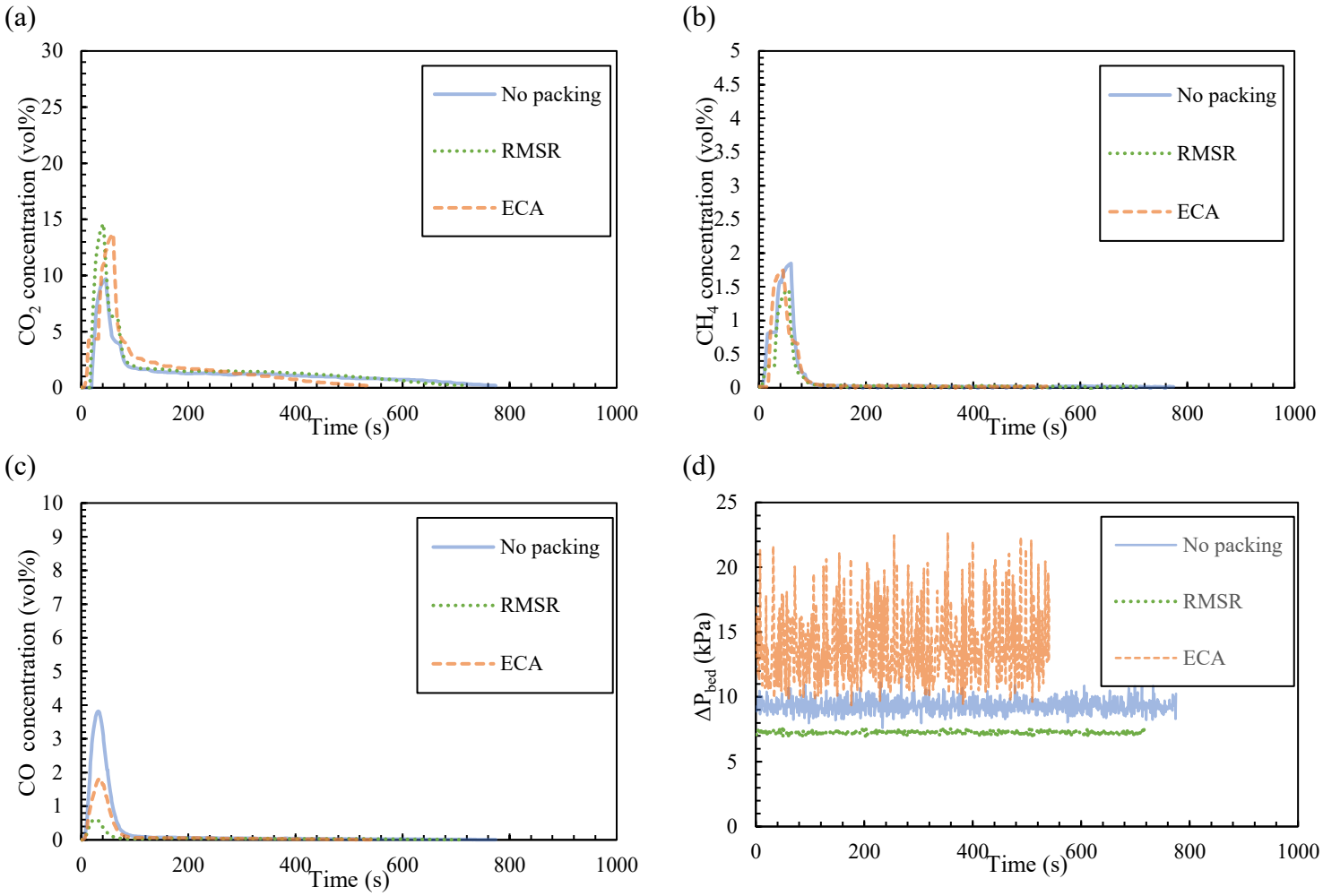

Figure 4.4. Outlet gas concentration and pressure profiles as a function of time for batch CLC experiments using torrefied wood pellet at a superficial gas velocity of 0.3 m/s and fuel reactor temperature of 900°C; comparing three bed configurations: No packing, RMSR, and ECA: (a) CO_2, (b) CH_4, (c) CO concentrations, and (d) bed pressure drop.

4.2 Carbon dioxide conversion yield

In this section, the carbon released as CO_2 and the total carbon in the gaseous products are first calculated using Equations 2-14 – 2-19 in the theory section. Based on these values, the CO_2 yield for each experimental run is determined using Equation 2-14. The results for the wood pellet experiments are summarized in Table 4.2, while those for the torrefied wood pellet are presented in Table 4.3. In the final column of Tables 4.2 and 4.3, the average CO_2 yield of all repetitions for each experimental condition is reported.

Table 4-5. Carbon released as CO_2, total carbon in gaseous products, and calculated CO_2 yield for wood pellet experiments at superficial gas velocities of 0.15 and 0.3 m/s under no-packing, RMSR, and ECA bed configurations.

Velocity (m/s)	Packings	Experiments	C in CO2(g)	Total Carbon(g)	CO2 yield (%)	Avg CO2 yield (%)
0.15	No packing	Run 1	0.64	0.88	72.6	73.0
		Run 2	0.64	0.90	71.8	
		Run 3	0.70	0.93	75.2	
		Run 4	0.65	0.90	72.6	
	RMSR	Run 1	0.90	0.99	91.3	91.8
		Run 2	0.86	0.94	91.5	
		Run 3	0.87	0.94	91.8	
		Run 4	0.87	0.94	92.7	
	ECA	Run 1	0.68	0.77	87.8	88.3
		Run 2	0.57	0.64	88.0	
		Run 3	0.64	0.72	88.8	
		Run 4	0.65	0.73	89.4	
		Run 5	0.82	0.94	87.5	
0.3	No packing	Run 1	0.73	0.99	73.7	73.0
		Run 2	0.74	1.00	74.3	
		Run 3	0.68	0.92	73.6	
		Run 4	0.68	0.94	71.7	
		Run 5	0.79	1.10	71.9	
	RMSR	Run 1	0.94	1.10	85.5	87.5
		Run 2	0.96	1.10	87.3	
		Run 3	0.94	1.07	87.9	
		Run 4	0.96	1.08	88.4	
		Run 5	0.95	1.08	88.5	
	ECA	Run 1	0.78	0.92	85.2	83.5
		Run 2	0.89	1.04	85.8	
		Run 3	0.85	1.00	84.8	
		Run 4	0.77	0.94	82.0	
		Run 5	0.86	1.06	80.8	
		Run 6	0.63	0.76	82.4	

As discussed in the previous section and shown in Table 4.2, the CO_2 yield for wood pellets increases when both packing materials are introduced compared to the no-packing configuration. This improvement is attributed to enhanced gas–solid contact and improved hydrodynamics due to bubble breakage and reduced bubble size. At a superficial gas velocity of 0.15 m/s, the average CO_2 yield increases from 73.0% in the no-packing case to 91.8% with RMSR and 88.3% with ECA.

Increasing the superficial gas velocity from 0.15 m/s to 0.3 m/s has only a minor effect on the no-packing configuration. However, in packed configurations, a slight decrease in CO_2 yield is observed at 0.3 m/s, which is mainly attributed to reduced gas residence time and stronger

dilution effects. For instance, for wood pellets with RMSR packing, the average CO_2 yield decreases from 91.8% at 0.15 m/s to 87.5% at 0.3 m/s.

The results in Table 4.2 also show that the CO_2 yield remains relatively stable across most repetitions. However, in the ECA configuration at 0.3 m/s, a gradual decrease in yield is observed with increasing experimental runs. This trend is likely associated with the loss of ECA material from the reactor system, as confirmed by post-experimental measurements. The initial ECA mass decreased from 381 g to 135.6 g after the first set of experiments with wood pellets. Before conducting the experiments with torrefied wood pellets, the bed was refilled with 381 g of ECA packing, which then decreased to 225.8 g after the experiments. Changes in the average pressure drop profile, presented in Table 7-5 and Table 7-66.6 in Appendix B, further support this observation.

A previous study by Aronsson et al. reported that ECA particles exhibit a floating regime at lower superficial velocities (around 0.18 m/s), while at higher velocities they become fully co-fluidized within the bed.[17] In the present study, 0.15 m/s corresponds to conditions close to the floating regime, whereas 0.3 m/s might lead to co-fluidization. This transition increases particle–particle and particle–wall interactions, which can enhance attrition and promote ECA loss. This interpretation is supported by experimental observations at 0.3 m/s, where particle collisions could be heard and dust emission from the reactor outlet was visually observed.

Similarly, Table 4.3 summarizes the calculated CO_2 yield for the torrefied wood pellet experiments under different operating conditions.

Table 4-6. Carbon released as CO_2, total carbon in gaseous products, and calculated CO_2 yield for torrefied wood pellet experiments at superficial gas velocities of 0.15 and 0.3 m/s under no-packing, RMSR, and ECA bed configurations.

Velocity (m/s)	Packings	Experiments	C in CO2(g)	Total Carbon(g)	CO2 yield (%)	Avg CO2 yield (%)
0.15	No packing	Run 1	0.88	1.10	80.1	80.8
		Run 2	0.88	1.08	81.3	
		Run 3	0.78	0.96	81.1	
		Run 4	0.91	1.11	81.7	
		Run 5	0.84	1.05	79.8	
	RMSR	Run 1	1.00	1.07	93.2	93.7
		Run 2	1.04	1.11	93.4	
		Run 3	0.89	0.96	93.6	
		Run 4	1.13	1.20	94.1	
		Run 5	1.08	1.14	94.2	
	ECA	Run 1	1.02	1.10	92.9	93.1
		Run 2	0.92	0.99	93.1	
		Run 3	0.97	1.04	92.8	
		Run 4	0.96	1.03	93.2	
		Run 5	0.96	1.03	93.4	
0.3	No packing	Run 1	0.94	1.17	80.4	79.7
		Run 2	0.99	1.24	79.6	
		Run 3	0.91	1.15	79.3	
		Run 4	1.01	1.28	78.6	
		Run 5	0.94	1.17	80.4	
	RMSR	Run 1	1.11	1.24	90.0	91.4
		Run 2	1.15	1.26	91.5	
		Run 3	1.20	1.30	92.1	
		Run 4	1.19	1.29	92.1	
	ECA	Run 1	1.07	1.20	88.9	86.4
		Run 2	1.08	1.24	86.9	
		Run 3	1.03	1.17	88.1	
		Run 4	1.05	1.20	87.4	
		Run 5	0.94	1.11	84.6	
		Run 6	0.90	1.10	82.4	

The CO_2 yield for torrefied wood pellets, as presented in Table 4.3, also increases when RMSR and ECA packings are introduced compared to the no-packing configuration. A comparison of Tables 4.2 and 4.3 shows that torrefied wood pellets consistently exhibit higher CO_2 conversion than wood pellets under all operating conditions, both with and without packing. This behavior can be attributed to its lower volatile matter content and higher fixed carbon fraction. For example, at a superficial gas velocity of 0.15 m/s under the no-packing configuration, the CO_2 yield increases from 73.0% for wood pellets to 80.8% for torrefied wood pellets. In the best case, the no-packing configuration does not exceed a CO_2 yield of 80.8%, whereas both RMSR and ECA configurations achieve values above 93%, indicating a significant improvement in conversion performance due to packing.

An increase in superficial gas velocity from 0.15 m/s to 0.3 m/s leads to a decrease in CO_2 yield for torrefied wood pellets under all configurations, including both packed and unpacked beds. This trend is consistent with reduced gas residence time and enhanced dilution effects at higher velocities.

The results in Table 4.3 further show that the CO_2 yield remains relatively stable across most repetitions. However, in the ECA configuration at 0.3 m/s, a gradual decrease in yield is again observed with increasing experimental repetitions, consistent with trends reported for wood pellets.

5 Conclusion

This study investigated the effect of packing materials on biomass conversion in a Chemical Looping Combustion process within a Packed-Fluidized Bed Reactor. Experiments were conducted using wood pellets and torrefied wood pellets as fuels, ilmenite as the oxygen carrier, and two packing materials RMSR and ECA at superficial gas velocities of 0.15 and 0.3 m/s temperature of 900°C. The key findings are summarized below:

RMSR outperformed ECA across all conditions, achieving average CO_2 yields of 91.8% and 87.5% at 0.15 and 0.3 m/s, respectively, for wood pellets. ECA achieved 88.3% and 83.5% under the same conditions. The no-packing configuration produced the lowest yields, averaging around 73% for wood pellets at both velocities.

Torrefied wood pellets consistently yielded higher CO_2 conversion than wood pellets under all configurations. This is due to their lower volatile content, which leads to a more moderate devolatilization rate, smaller bubble formation during this stage, and improved gas–solid contact. However, their higher fixed carbon content results in significantly longer combustion times due to slower char gasification kinetics.

Increasing the superficial gas velocity from 0.15 to 0.3 m/s generally reduced CO_2 yield in packed configurations. This is explained by shorter gas residence times, larger bubble formation, and dilution of combustible species at higher gas flow rates. The no-packing configuration showed minimal sensitivity to velocity change.

ECA packing suffered material losses at 0.3 m/s, transitioning from a floating regime to co-fluidization with the ilmenite bed, which enhanced attrition and particle elutriation. This resulted in a gradual decline in CO_2 yield across repeated experimental runs at this velocity and represents a practical limitation of ECA packing at higher fluidization velocities.

In conclusion, RMSR packing at 0.15 m/s with torrefied wood pellets achieved the best overall performance, with an average CO_2 yield of 93.7%. These results demonstrate that introducing structured packing into fluidized bed CLC reactors is an effective strategy for improving fuel conversion efficiency.

6 Bibliography

[1] A. Omri and S. Boubaker, “When do climate change legislation and clean energy policies matter for net-zero emissions?,” *J. Environ. Manage.*, vol. 354, p. 120275, 2024, doi: https://doi.org/10.1016/j.jenvman.2024.120275.

[2] M. N. Anwar *et al.*, “Sources of Carbon Dioxide and Environmental Issues,” in *Sustainable Agriculture Reviews 37: Carbon Sequestration Vol. 1 Introduction and Biochemical Methods*, Inamuddin, A. M. Asiri, and E. Lichtfouse, Eds., Cham: Springer International Publishing, 2019, pp. 13–36. doi: 10.1007/978-3-030-29298-0_2.

[3] P. Friedlingstein *et al.*, “Global Carbon Budget 2024,” *Earth Syst. Sci. Data*, vol. 17, no. 3, pp. 965–1039, 2025, doi: 10.5194/essd-17-965-2025.

[4] “IEA (2021), Net Zero by 2050, IEA, Paris https://www.iea.org/reports/net-zero-by-2050, Licence: CC BY 4.0”.

[5] H. Zhao *et al.*, “Chemical looping combustion: Advantages, disadvantages, opportunities and challenges,” *The Innovation Energy*, vol. 2, no. 4, p. 100118, 2025, doi: 10.59717/j.xinn-energy.2025.100118.

[6] A. Lyngfelt, “Chemical Looping Combustion: Status and Development Challenges,” *Energy & Fuels*, vol. 34, no. 8, pp. 9077–9093, Aug. 2020, doi: 10.1021/acs.energyfuels.0c01454.

[7] D. Kunii and O. Levenspiel, *Fluidization Engineering*, 2nd ed. Boston: Butterworth-Heinemann, 1991.

[8] P. Peltola, F. Alobaid, T. Tynjälä, and J. Ritvanen, “Overview of Fluidized Bed Reactor Modeling for Chemical Looping Combustion: Status and Research Needs,” *Energy & Fuels*, vol. 36, no. 17, pp. 9385–9409, Sep. 2022, doi: 10.1021/acs.energyfuels.2c01680.

[9] S. Iannello, D. Macrì, and M. Materazzi, “A comprehensive assessment of endogenous bubbles properties in fluidized bed reactors via X-ray imaging,” *Powder Technol.*, vol. 413, p. 118013, 2023, doi: https://doi.org/10.1016/j.powtec.2022.118013.

[10] N. Nemati, Y. Tsuji, T. Mattisson, and M. Rydén, “Chemical Looping Combustion in a Packed Fluidized Bed Reactor─Fundamental Modeling and Batch Experiments with Random Metal Packings,” *Energy & Fuels*, vol. 36, no. 17, pp. 9538–9550, Sep. 2022, doi: 10.1021/acs.energyfuels.2c00527.

[11] R. Munnoch, “‘Introduction to Particle Technology’: By Martin Rhodes (Monash University, Australia) and Jonathan Seville (University of Birmingham, UK), John Wiley & Sons Ltd, Chichester, West Sussex, UK, 2024, 496 pp, ISBN: 978-1-119-93110-2, £67.40, €81.39, US$84.95,” *Johnson Matthey Technology Review*, vol. 69, pp. 321–326, Apr. 2025, doi: 10.1595/205651325X17400462250217.

[12] A. Abad, Ó. Condori, L. F. de Diego, and F. García-Labiano, “Determining Intrinsic Biomass Gasification Kinetics and Its Application on Gasification of Pelletized Biomass: Simplifying the Process for Use in Chemical Looping Processes,” *Fire*, vol. 9, no. 1, 2026, doi: 10.3390/fire9010009.

[13] J. Aronsson, E. Krymarys, V. Stenberg, T. Mattisson, A. Lyngfelt, and M. Rydén, “Improved Gas–Solids Mass Transfer in Fluidized Beds: Confined Fluidization in Chemical-Looping Combustion,” *Energy & Fuels*, vol. 33, no. 5, pp. 4442–4453, May 2019, doi: 10.1021/acs.energyfuels.9b00508.

[14] A. M. Rashad, “Lightweight expanded clay aggregate as a building material – An overview,” *Constr. Build. Mater.*, vol. 170, pp. 757–775, 2018, doi: https://doi.org/10.1016/j.conbuildmat.2018.03.009.

[15] M. Keller, H. Leion, T. Mattisson, and A. Lyngfelt, “Gasification inhibition in chemical-looping combustion with solid fuels,” *Combust. Flame*, vol. 158, no. 3, pp. 393–400, 2011, doi: https://doi.org/10.1016/j.combustflame.2010.09.009.

[16] S. Sadjadi, U. Simon, H. R. Godini, O. Görke, R. Schomäcker, and G. Wozny, “Reactor Material and Gas Dilution Effects on the Performance of Miniplant-Scale Fluidized-Bed Reactors for Oxidative Coupling of Methane,” *Chemical Engineering Journal*, vol. 281, pp. 678–687, Dec. 2015, doi: 10.1016/j.cej.2015.06.079.

[17] J. Aronsson, D. Pallarès, M. Rydén, and A. Lyngfelt, “Increasing Gas–Solids Mass Transfer in Fluidized Beds by Application of Confined Fluidization—A Feasibility Study,” *Applied Sciences*, vol. 9, p. 634, Feb. 2019, doi: 10.3390/app9040634.

7 Appendix

7.1 Appendix A

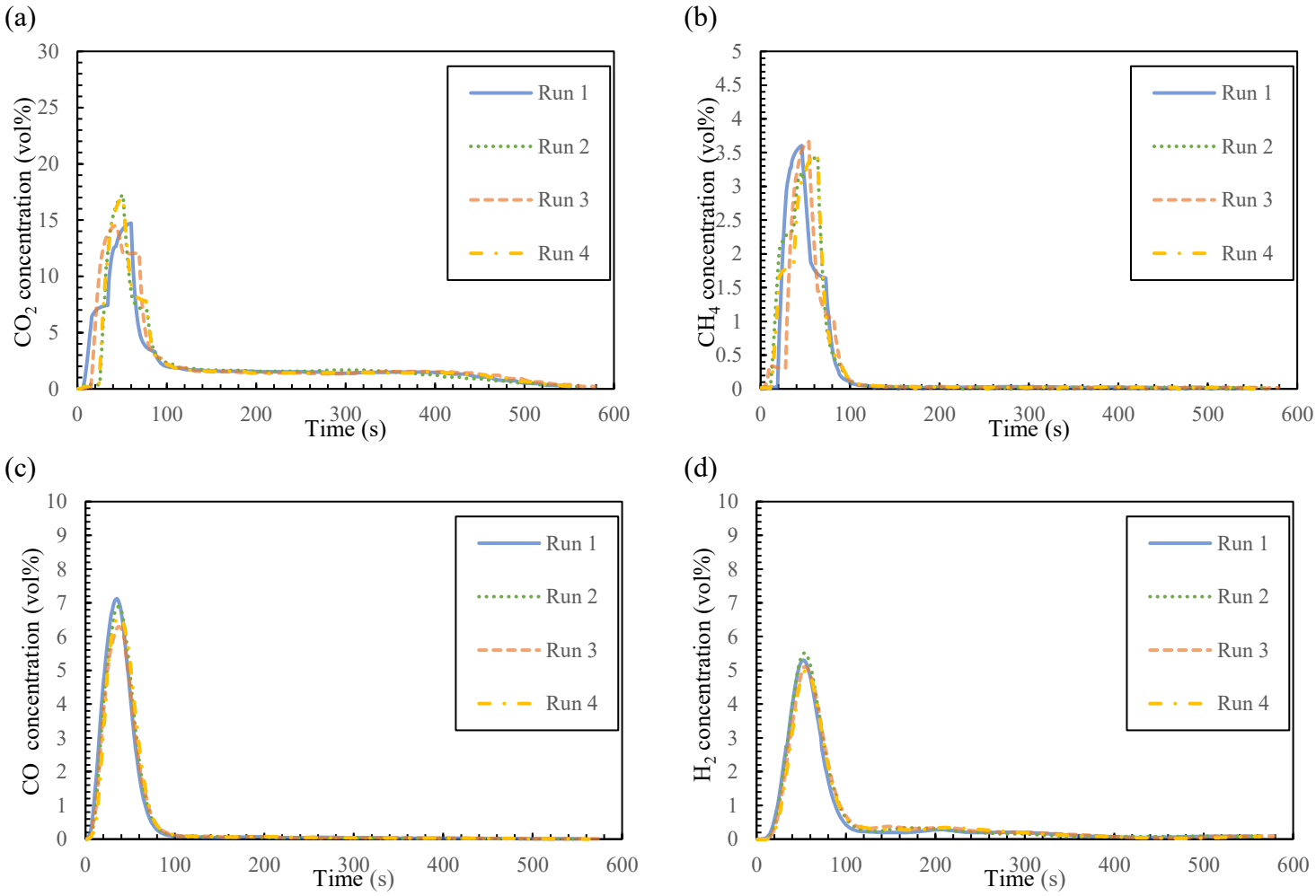

Figure 7.1. Outlet gas concentration profiles as a function of time for batch CLC experiments using wood pellet with no packing configuration at a superficial gas velocity of 0.15 m/s and fuel reactor temperature of 900°C; comparing different experiment runs:(a) CO_2, (b) CH_4, (c) CO, and (d) H_2 concentrations.

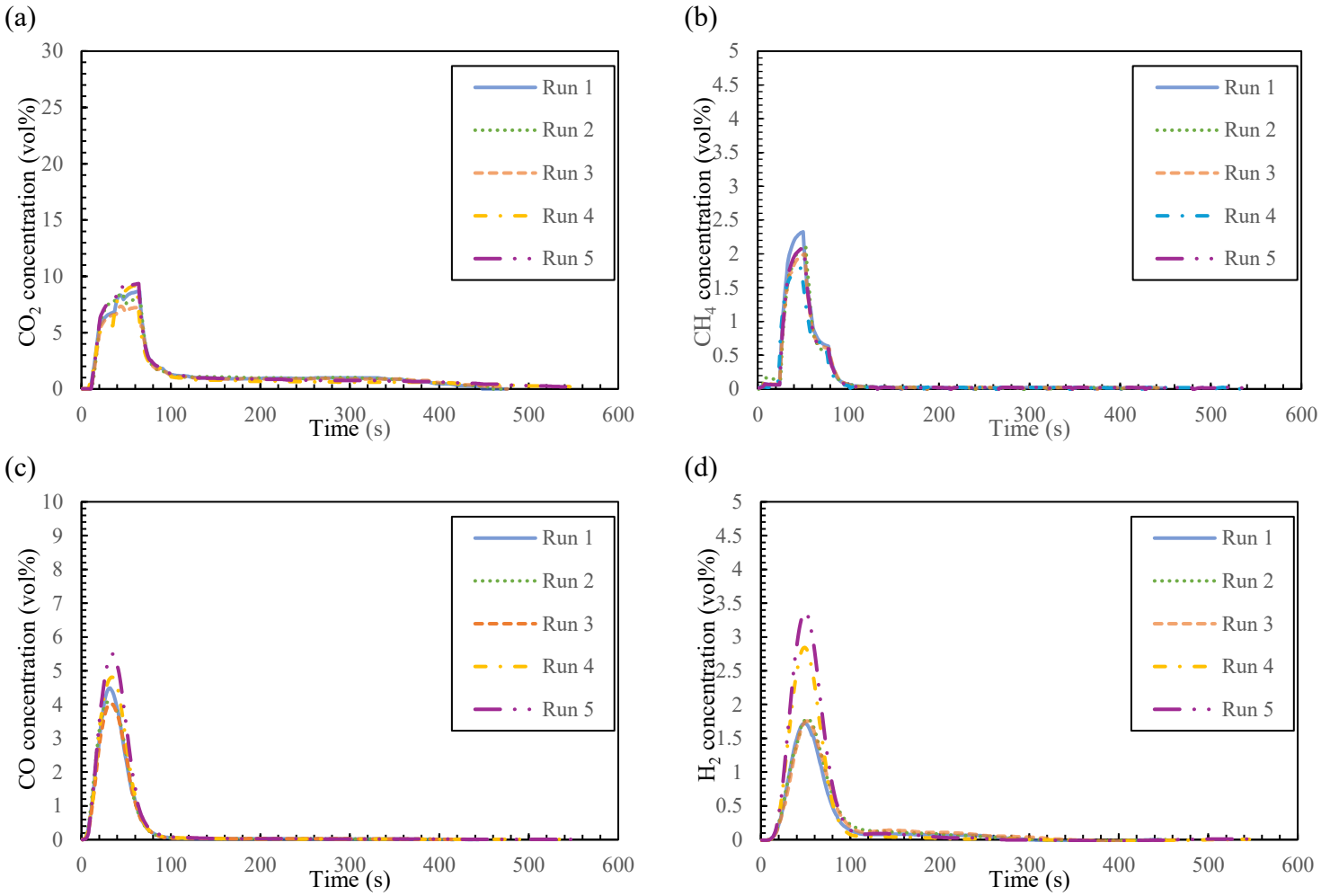

Figure 7.2. Outlet gas concentration profiles as a function of time for batch CLC experiments using wood pellet with no packing configuration at a superficial gas velocity of 0.3 m/s and fuel reactor temperature of 900°C; comparing different experiment runs:(a) CO_2, (b) CH_4, (c) CO, and (d) H_2 concentrations.

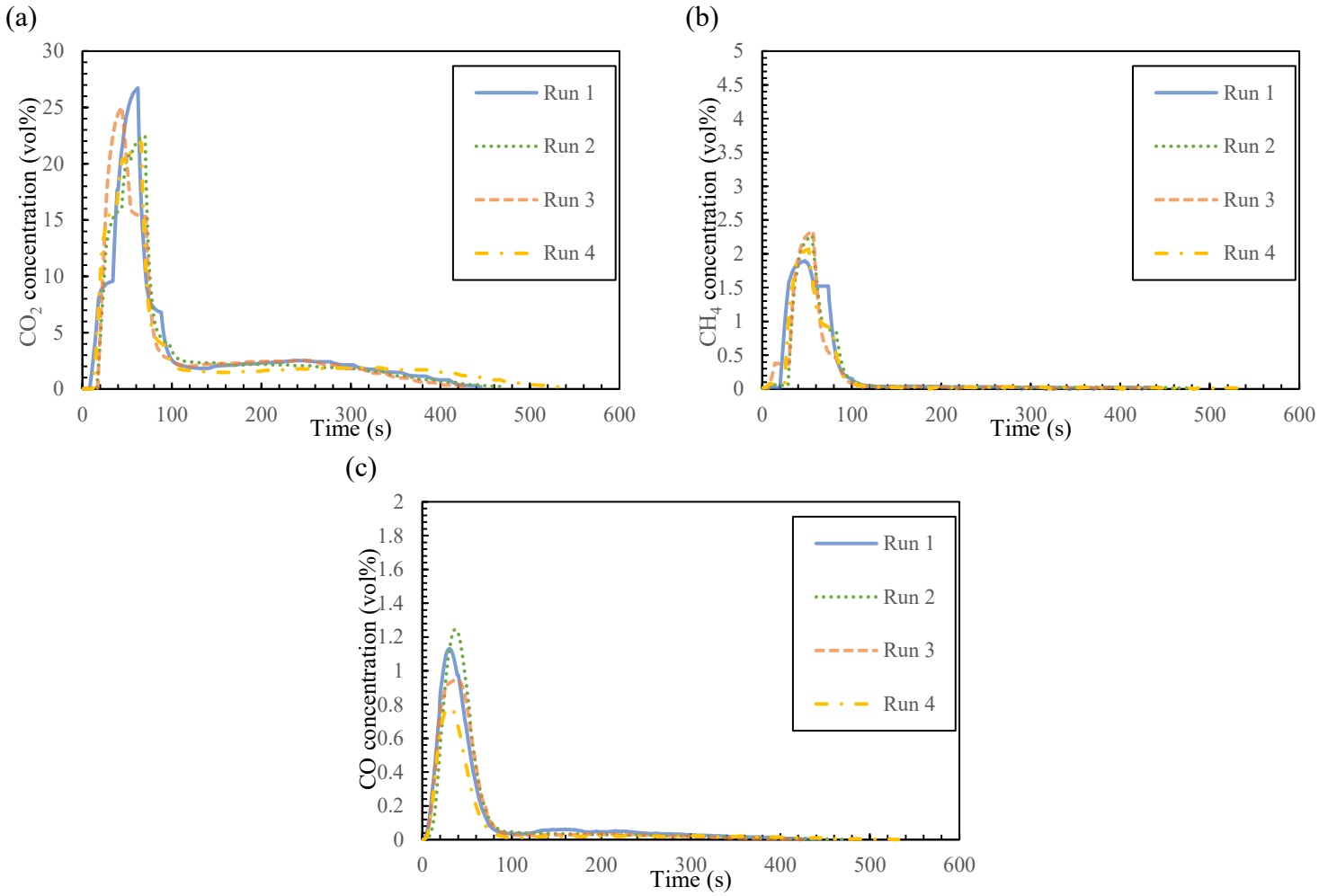

Figure 7.3. Outlet gas concentration profiles as a function of time for batch CLC experiments using wood pellet with RMSR at a superficial gas velocity of 0.15 m/s and fuel reactor temperature of 900°C; comparing different experiment runs:(a) CO_2, (b) CH_4, (c) CO, and (d) H_2 concentrations.

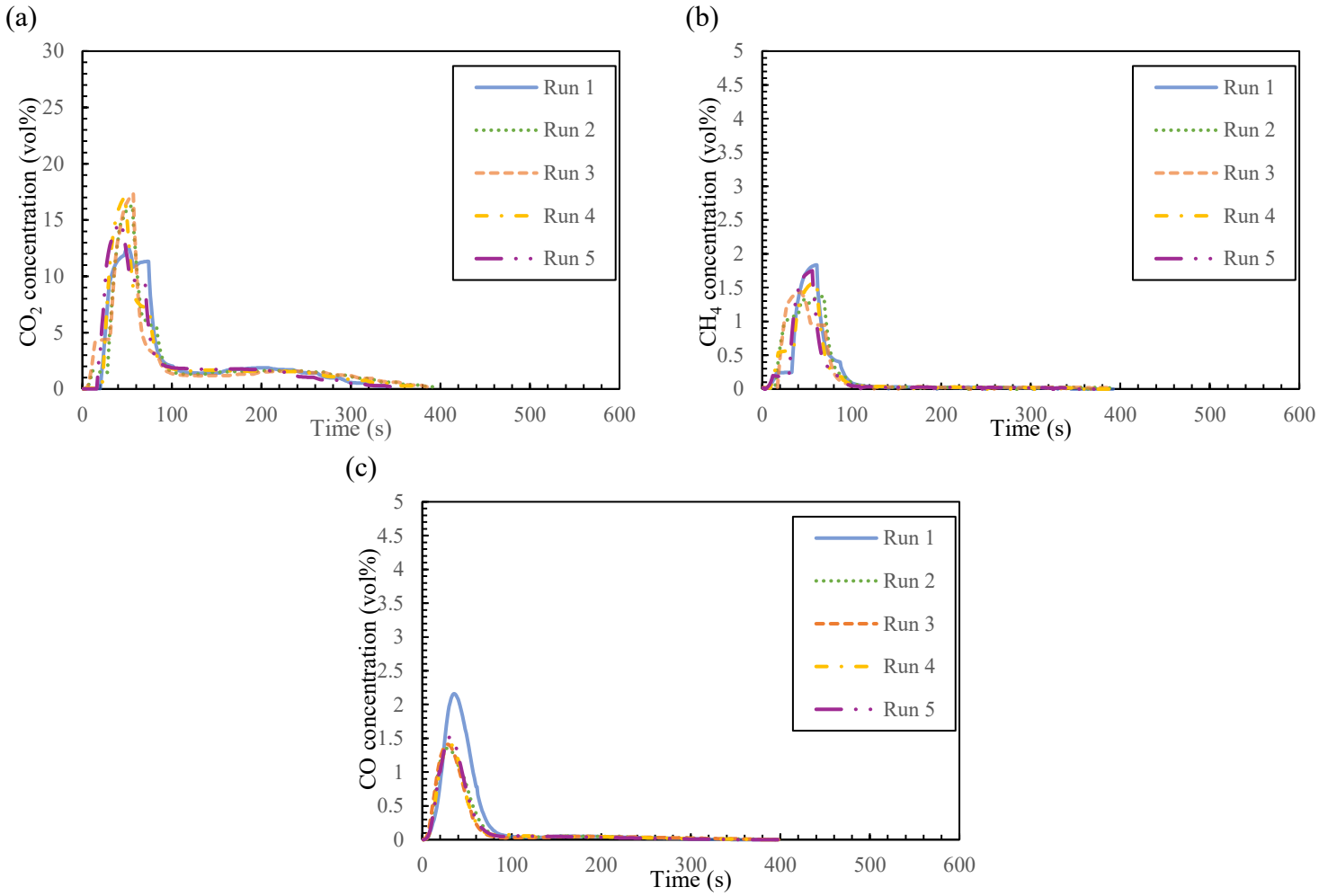

Figure 7.4. Outlet gas concentration profiles as a function of time for batch CLC experiments using wood pellet with RMSR at a superficial gas velocity of 0.3 m/s and fuel reactor temperature of 900°C; comparing different experiment runs:(a) CO_2, (b) CH_4, (c) CO, and (d) H_2 concentrations.

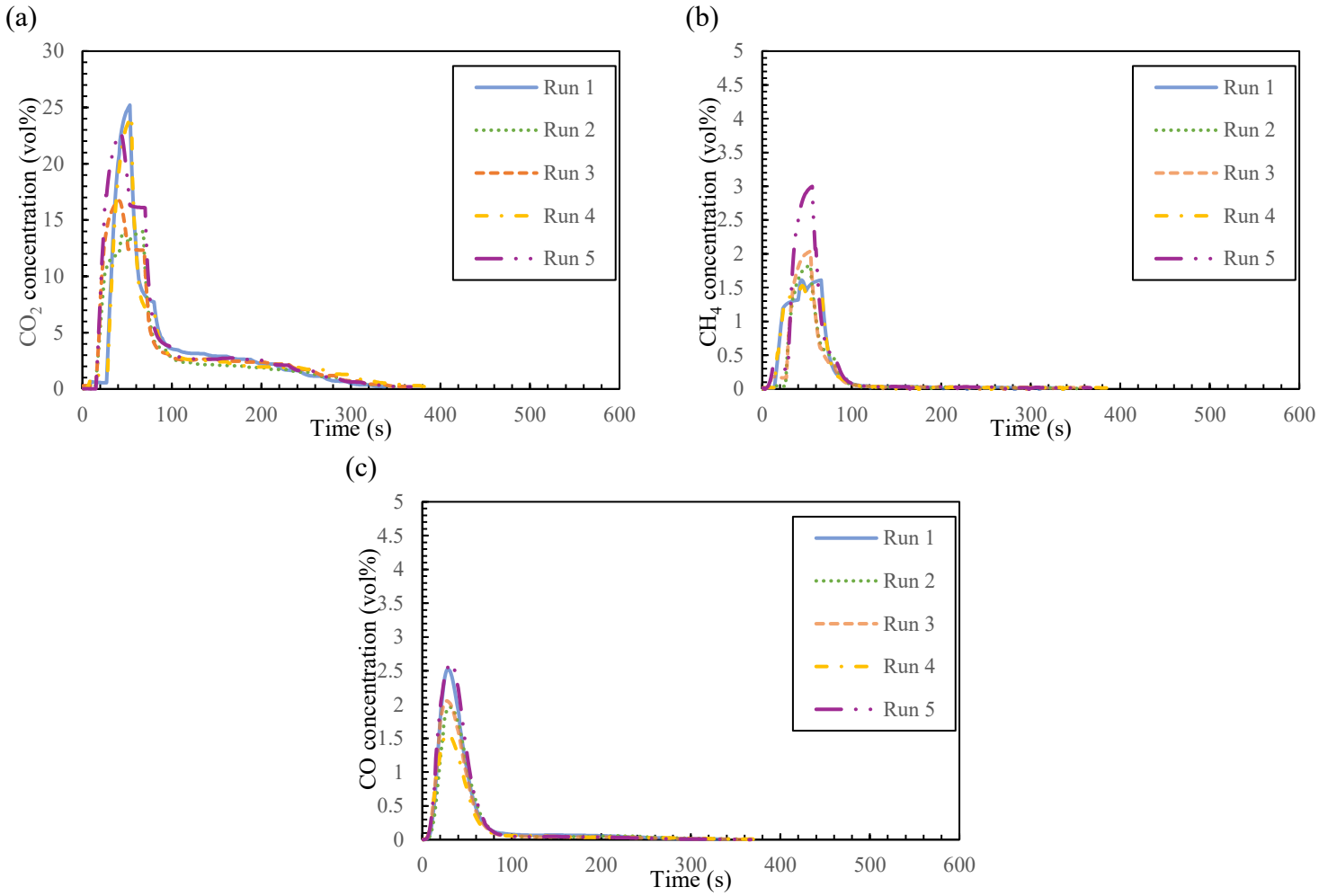

Figure 7.5. Outlet gas concentration profiles as a function of time for batch CLC experiments using wood pellet with ECA at a superficial gas velocity of 0.15 m/s and fuel reactor temperature of 900°C; comparing different experiment runs:(a) CO_2, (b) CH_4, (c) CO, and (d) H_2 concentrations.

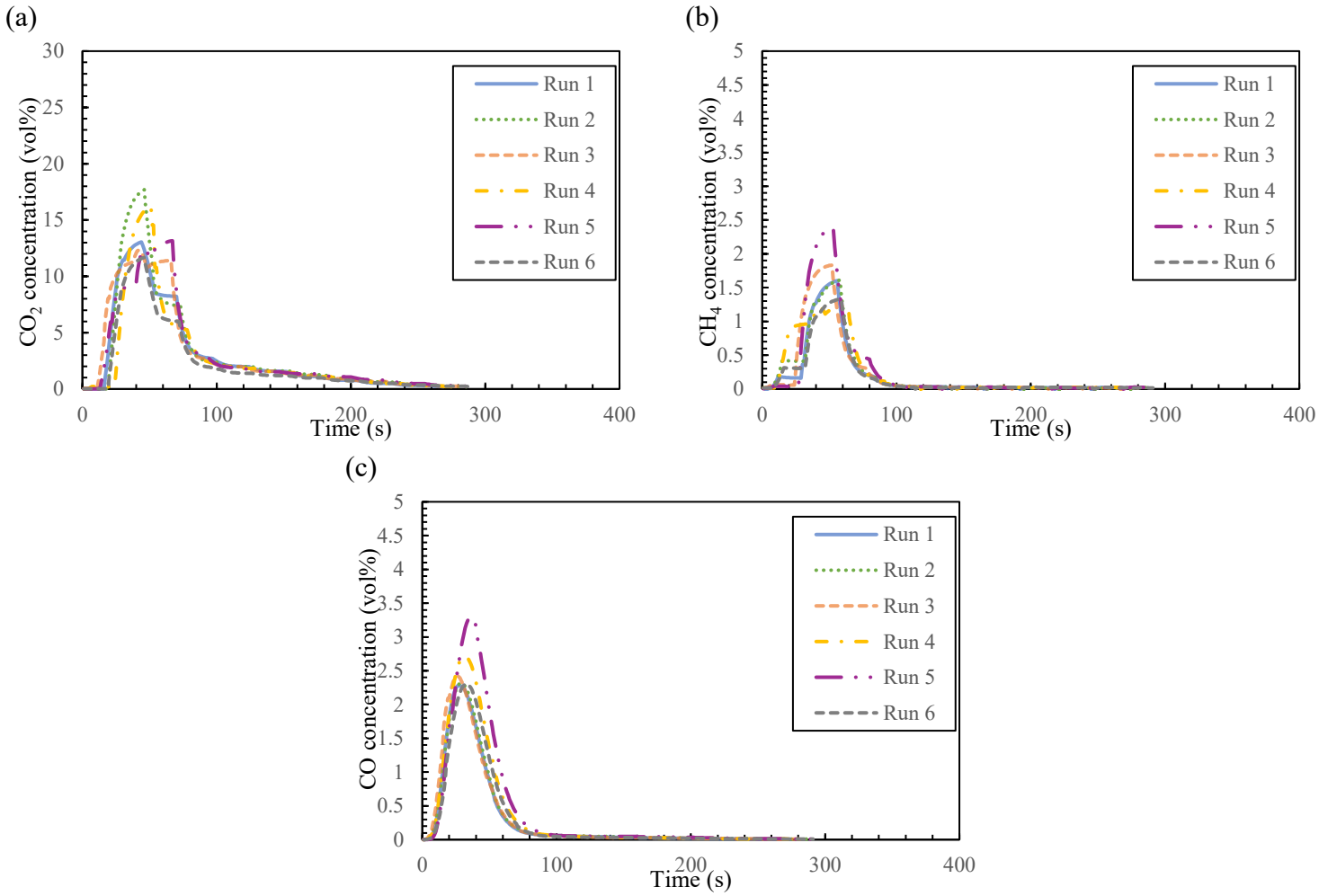

Figure 7.6. Outlet gas concentration profiles as a function of time for batch CLC experiments using wood pellet with ECA at a superficial gas velocity of 0.3 m/s and fuel reactor temperature of 900°C; comparing different experiment runs:(a) CO_2, (b) CH_4, (c) CO, and (d) H_2 concentrations.

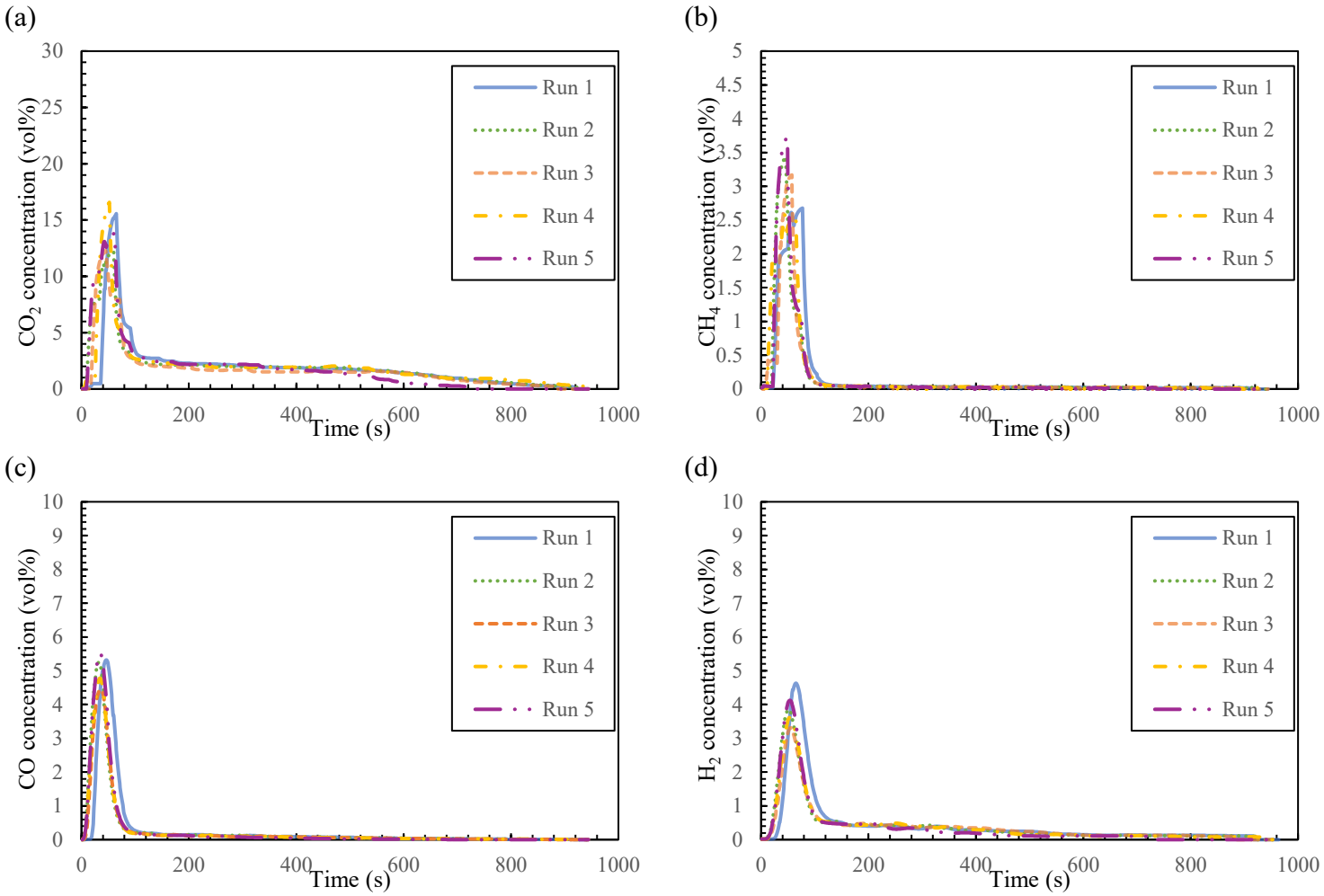

Figure 7.7. Outlet gas concentration profiles as a function of time for batch CLC experiments using torrefied wood with no packing configuration at a superficial gas velocity of 0.15 m/s and fuel reactor temperature of 900°C; comparing different experiment runs:(a) CO_2, (b) CH_4, (c) CO, and (d) H_2 concentrations.

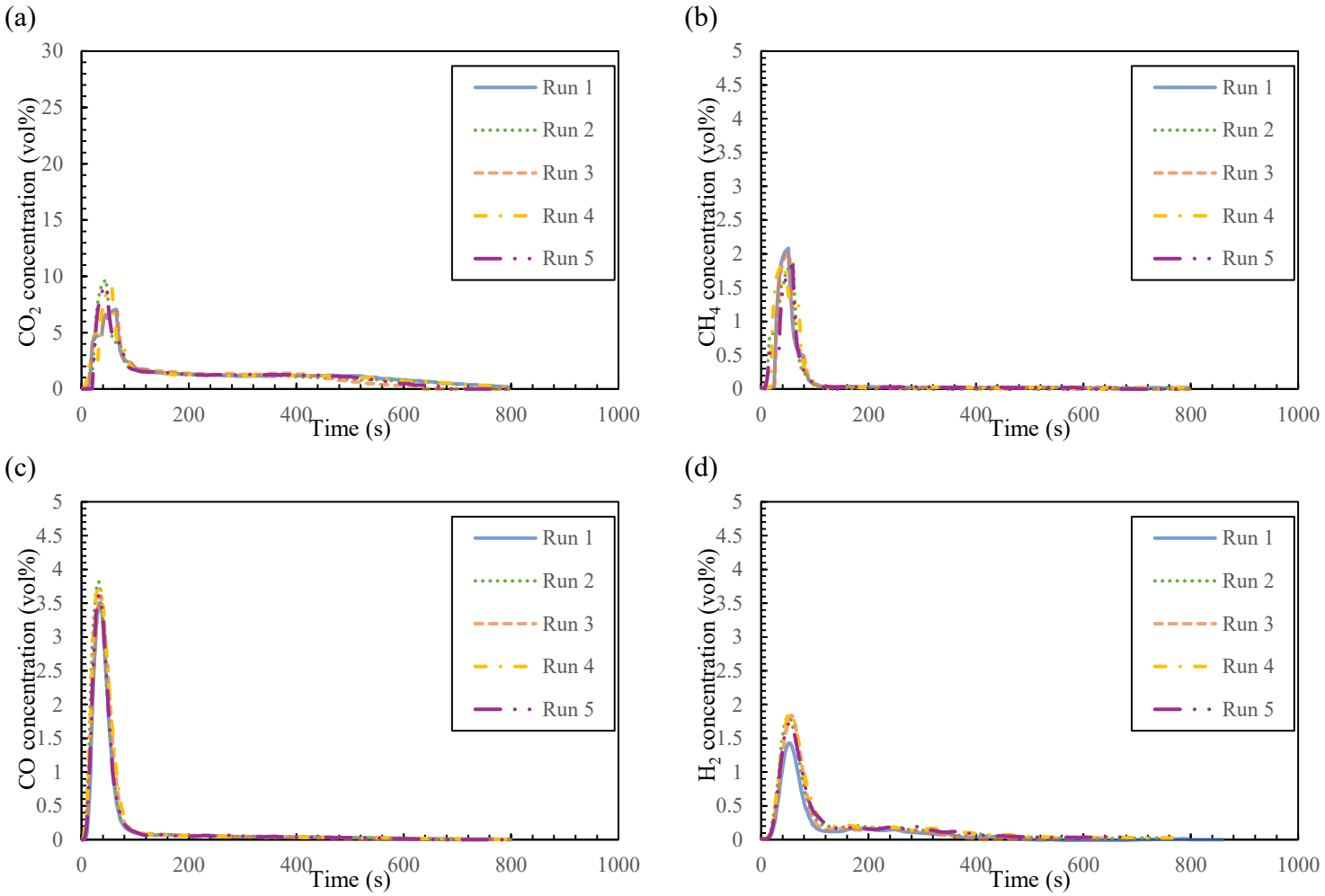

Figure 7.8. Outlet gas concentration profiles as a function of time for batch CLC experiments using torrefied wood with no packing configuration at a superficial gas velocity of 0.3 m/s and fuel reactor temperature of 900°C; comparing different experiment runs:(a) CO_2, (b) CH_4, (c) CO, and (d) H_2 concentrations.

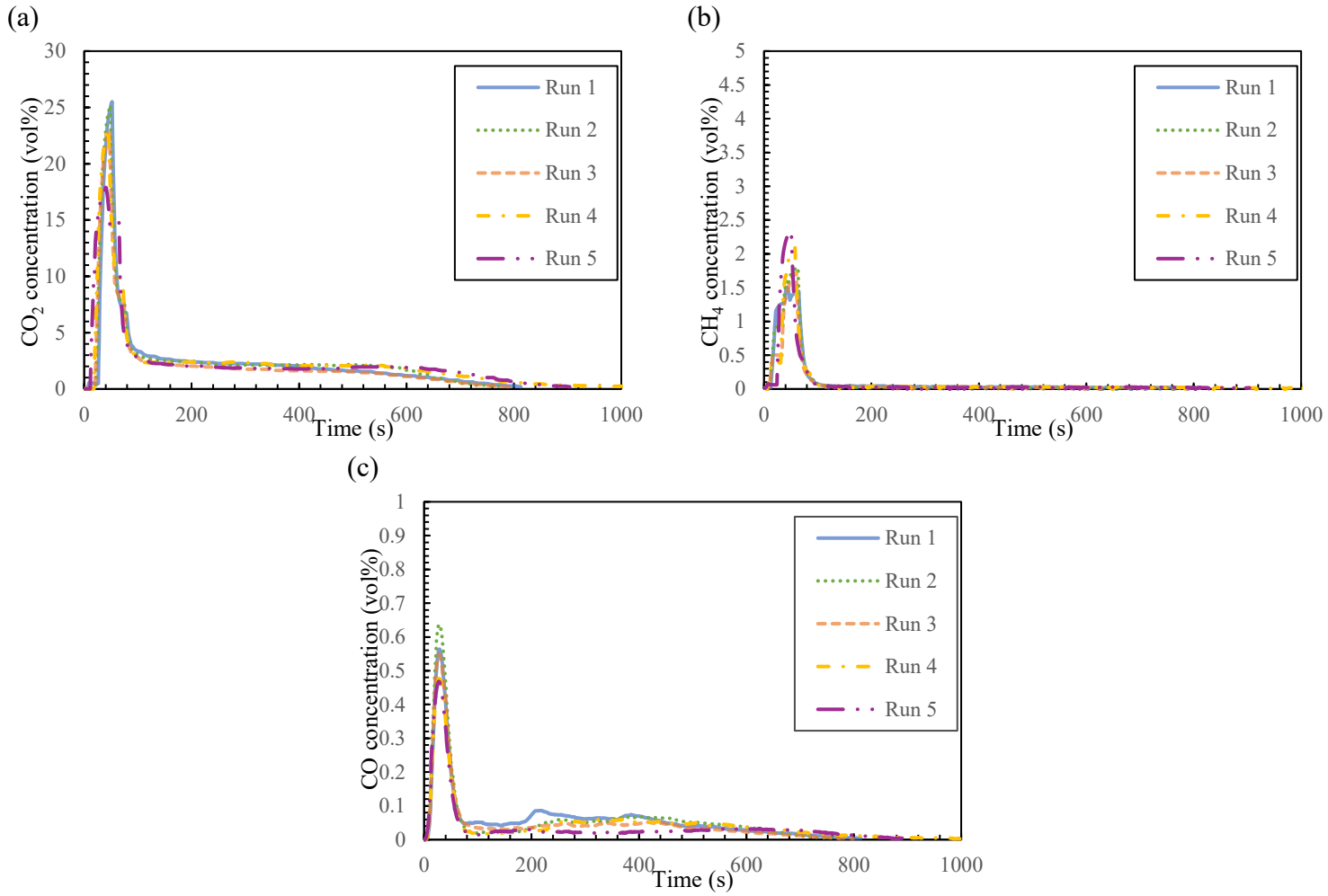

Figure 7.9. Outlet gas concentration profiles as a function of time for batch CLC experiments using torrefied wood with RMSR at a superficial gas velocity of 0.15 m/s and fuel reactor temperature of 900°C; comparing different experiment runs:(a) CO_2, (b) CH_4, (c) CO, and (d) H_2 concentrations.

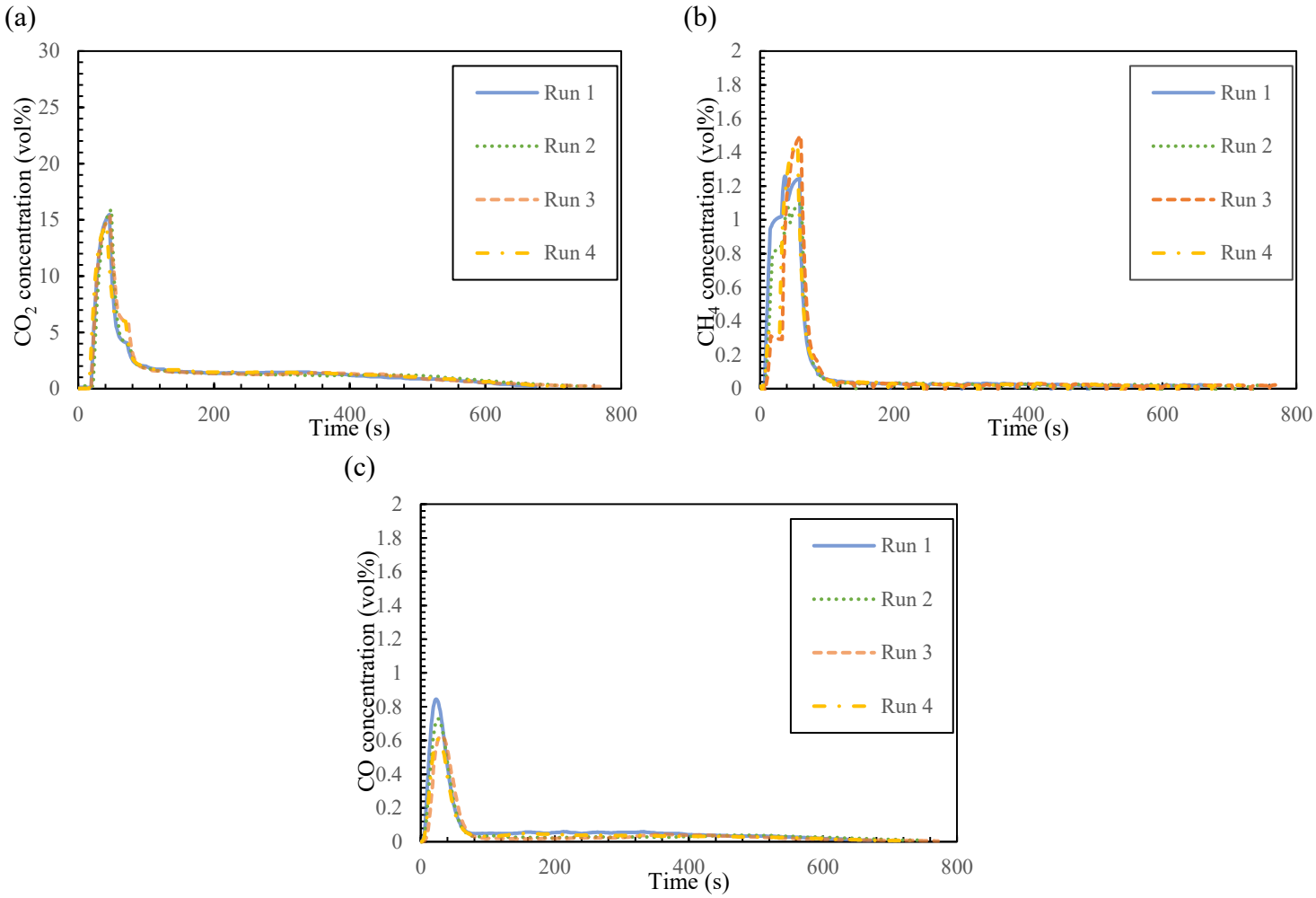

Figure 7.10. Outlet gas concentration profiles as a function of time for batch CLC experiments using torrefied wood with RMSR at a superficial gas velocity of 0.3 m/s and fuel reactor temperature of 900°C; comparing different experiment runs:(a) CO_2, (b) CH_4, (c) CO, and (d) H_2 concentrations.

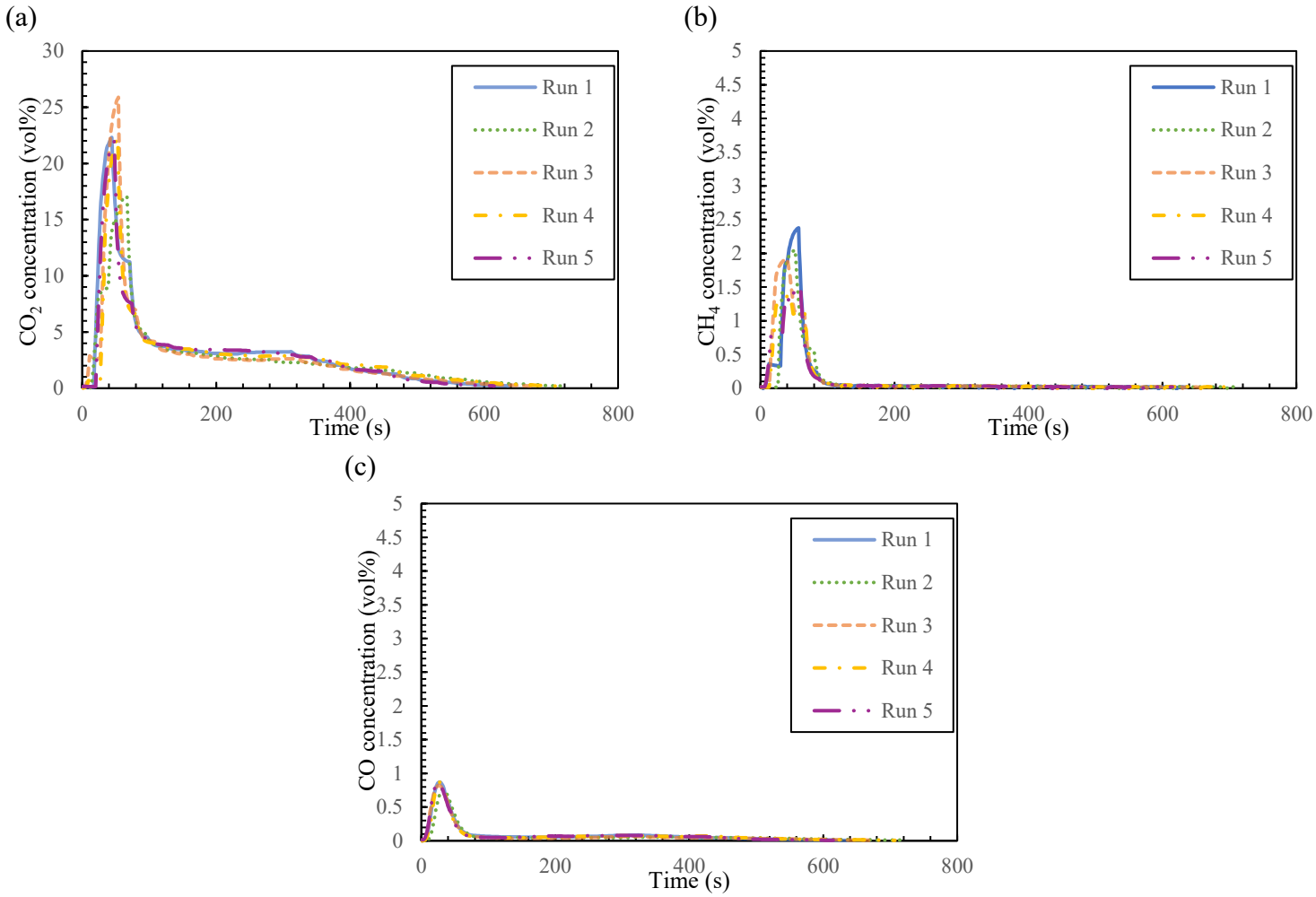

Figure 7.11. Outlet gas concentration profiles as a function of time for batch CLC experiments using torrefied wood with ECA at a superficial gas velocity of 0.15 m/s and fuel reactor temperature of 900°C; comparing different experiment runs:(a) CO_2, (b) CH_4, (c) CO, and (d) H_2 concentrations.

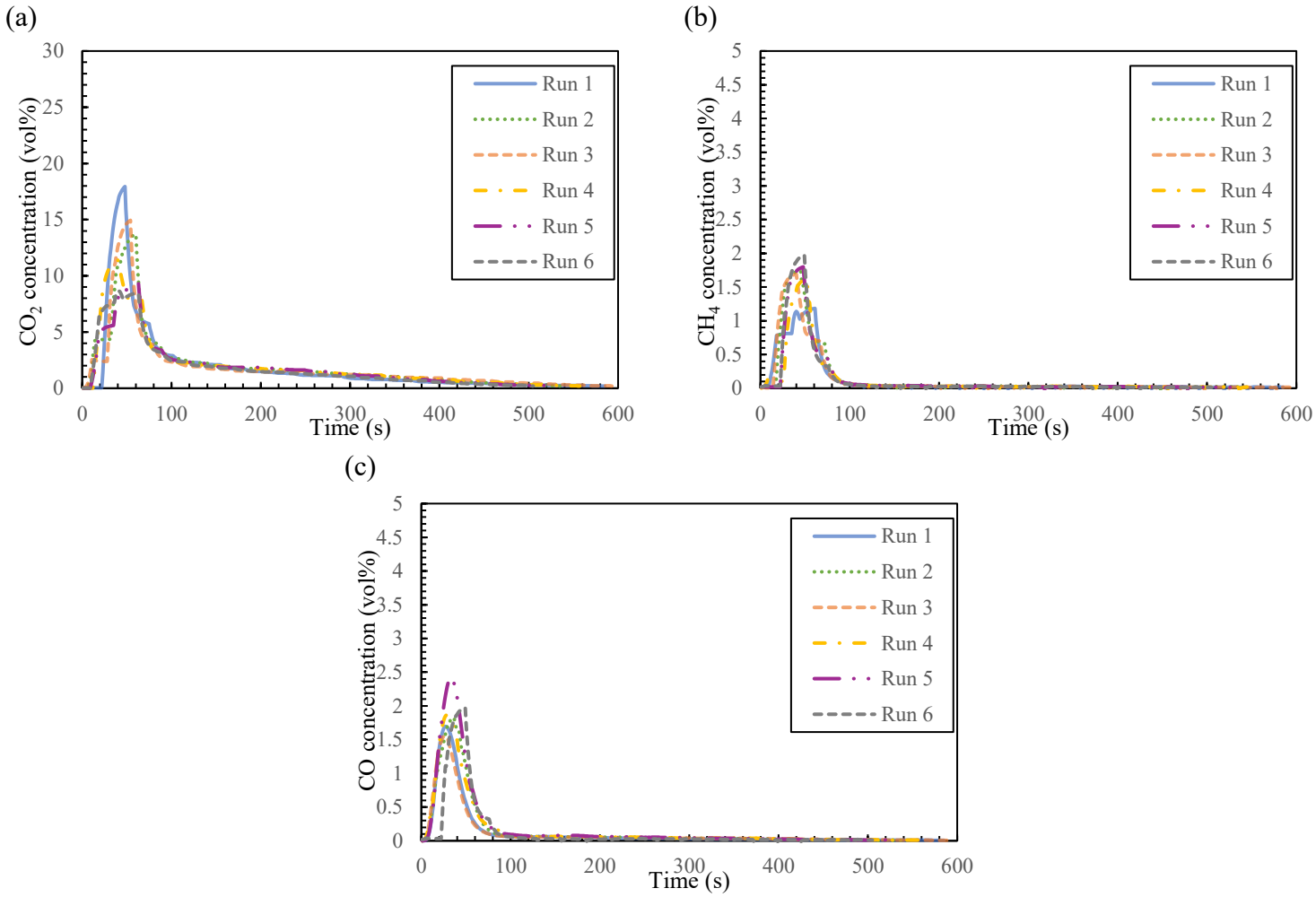

Figure 7.12. Outlet gas concentration profiles as a function of time for batch CLC experiments using torrefied wood with ECA at a superficial gas velocity of 0.3 m/s and fuel reactor temperature of 900°C; comparing different experiment runs:(a) CO_2, (b) CH_4, (c) CO, and (d) H_2 concentrations.

7.2 Appendix B

Table 7-1. Volumetric fractions of outlet gases (Excluding N_2) for each experiment run using wood pellets at superficial velocities of 0.15 and 0.3 m/s under three bed configurations: no packing, RMSR, and ECA.

Velocity (m/s)	Packings	Experiments	yCO2 (-)	yCH4 (-)	yCO (-)	yH2 (-)
0.15	No packing	Run 1	0.633	0.077	0.141	0.149
		Run 2	0.618	0.086	0.139	0.157
		Run 3	0.653	0.069	0.128	0.150
		Run 4	0.631	0.081	0.139	0.148
		Average	0.634	0.079	0.137	0.151
	RMSR	Run 1	0.915	0.056	0.029	0.000
		Run 2	0.918	0.052	0.029	0.000
		Run 3	0.921	0.052	0.028	0.000
		Run 4	0.930	0.050	0.020	0.000
		Average	0.921	0.053	0.026	0.000
	ECA	Run 1	0.879	0.059	0.063	0.000
		Run 2	0.883	0.055	0.062	0.000
		Run 3	0.892	0.053	0.056	0.000
		Run 4	0.894	0.059	0.047	0.000
		Run 5	0.881	0.062	0.057	0.000
		Average	0.886	0.057	0.057	0.000
0.3	No packing	Run 1	0.688	0.081	0.154	0.077
		Run 2	0.686	0.075	0.153	0.087
		Run 3	0.675	0.077	0.155	0.093
		Run 4	0.647	0.070	0.174	0.109
		Run 5	0.644	0.067	0.172	0.118
		Average	0.668	0.074	0.162	0.097
	RMSR	Run 1	0.858	0.065	0.077	0.000
		Run 2	0.874	0.070	0.056	0.000
		Run 3	0.880	0.066	0.054	0.000
		Run 4	0.885	0.062	0.053	0.000
		Run 5	0.887	0.058	0.055	0.000
		Average	0.877	0.064	0.059	0.000
	ECA	Run 1	0.855	0.060	0.085	0.000
		Run 2	0.859	0.060	0.081	0.000
		Run 3	0.851	0.064	0.084	0.000
		Run 4	0.820	0.071	0.108	0.000
		Run 5	0.812	0.075	0.112	0.000
		Run 6	0.827	0.066	0.107	0.000
		Average	0.838	0.066	0.096	0.000

Table 7-2. Volumetric fractions of outlet gases (Excluding N_2) for each experiment run using torrefied wood at superficial velocities of 0.15 and 0.3 m/s under three bed configurations: no packing, RMSR, and ECA.

Velocity (m/s)	Packings	Experiments	yCO2 (-)	yCH4 (-)	yCO (-)	yH2 (-)
0.15	No packing	Run 1	0.687	0.059	0.099	0.155
		Run 2	0.705	0.054	0.096	0.146
		Run 3	0.694	0.055	0.096	0.156
		Run 4	0.711	0.059	0.089	0.141
		Run 5	0.700	0.060	0.102	0.139
		Average	0.699	0.057	0.096	0.147
	RMSR	Run 1	0.933	0.044	0.023	0.000
		Run 2	0.936	0.043	0.021	0.000
		Run 3	0.937	0.042	0.021	0.000
		Run 4	0.943	0.039	0.018	0.000
		Run 5	0.945	0.040	0.015	0.000
		Average	0.939	0.042	0.020	0.000
	ECA	Run 1	0.932	0.043	0.025	0.000
		Run 2	0.933	0.043	0.025	0.000
		Run 3	0.929	0.047	0.024	0.000
		Run 4	0.933	0.041	0.027	0.000
		Run 5	0.935	0.038	0.027	0.000
		Average	0.932	0.042	0.026	0.000
0.3	No packing	Run 1	0.765	0.061	0.103	0.071
		Run 2	0.724	0.063	0.113	0.100
		Run 3	0.726	0.062	0.118	0.093
		Run 4	0.709	0.066	0.118	0.107
		Run 5	0.726	0.058	0.111	0.105
		Average	0.730	0.062	0.113	0.095
	RMSR	Run 1	0.901	0.059	0.039	0.000
		Run 2	0.916	0.053	0.032	0.000
		Run 3	0.922	0.050	0.027	0.000
		Run 4	0.922	0.049	0.029	0.000
		Average	0.916	0.053	0.032	0.000
	ECA	Run 1	0.890	0.054	0.056	0.000
		Run 2	0.872	0.062	0.066	0.000
		Run 3	0.883	0.062	0.056	0.000
		Run 4	0.878	0.052	0.070	0.000
		Run 5	0.851	0.061	0.089	0.000
		Run 6	0.830	0.063	0.107	0.000
		Average	0.867	0.059	0.074	0.000

Table 7-3. Mass of each outlet gas, mass of carbon in each outlet gas, total mass of carbon in outlet gases, and CO_2 yield for each experiment run using wood pellets at superficial velocities of 0.15 and 0.3 m/s under three bed configurations: no packing, RMSR, and ECA.

Velocity (m/s)	Packings	Experiments	CO2(g)	CH4(g)	CO(g)	C in CO2(g)	C in CH4 (g)	C in CO (g)	Total (g)	CO2 yield (%)	Avg CO2 yield (%)
0.15	No packing	Run 1	2.354	0.115	0.366	0.642	0.086	0.157	0.885	72.6	73.0
		Run 2	2.363	0.129	0.366	0.644	0.097	0.157	0.898	71.8	
		Run 3	2.568	0.109	0.349	0.700	0.081	0.149	0.931	75.2	
		Run 4	2.383	0.120	0.362	0.650	0.090	0.155	0.895	72.6	
	RMSR	Run 1	3.308	0.076	0.066	0.902	0.057	0.028	0.988	91.3	91.8
		Run 2	3.165	0.069	0.066	0.863	0.052	0.028	0.943	91.5	
		Run 3	3.177	0.068	0.062	0.866	0.051	0.027	0.944	91.8	
		Run 4	3.203	0.066	0.044	0.874	0.050	0.019	0.942	92.7	
	ECA	Run 1	2.480	0.061	0.112	0.676	0.046	0.048	0.770	87.8	88.3
		Run 2	2.073	0.049	0.095	0.565	0.037	0.041	0.643	88.0	
		Run 3	2.351	0.053	0.097	0.641	0.039	0.042	0.722	88.8	
		Run 4	2.378	0.058	0.078	0.649	0.044	0.033	0.726	89.4	
		Run 5	3.011	0.082	0.130	0.821	0.061	0.056	0.938	87.5	
0.3	No packing	Run 1	2.684	0.120	0.400	0.732	0.090	0.172	0.993	73.7	73.0
		Run 2	2.713	0.112	0.401	0.740	0.084	0.172	0.996	74.3	
		Run 3	2.482	0.107	0.378	0.677	0.080	0.162	0.919	73.6	
		Run 4	2.481	0.102	0.446	0.677	0.076	0.191	0.944	71.7	
		Run 5	2.894	0.115	0.520	0.789	0.086	0.223	1.098	71.9	
	RMSR	Run 1	3.460	0.098	0.202	0.944	0.074	0.087	1.104	85.5	87.5
		Run 2	3.519	0.105	0.143	0.960	0.079	0.061	1.100	87.3	
		Run 3	3.451	0.096	0.135	0.941	0.072	0.058	1.071	87.9	
		Run 4	3.513	0.091	0.135	0.958	0.068	0.058	1.084	88.4	
		Run 5	3.489	0.085	0.140	0.952	0.064	0.060	1.076	88.5	
	ECA	Run 1	2.869	0.074	0.186	0.783	0.056	0.080	0.918	85.2	83.5
		Run 2	3.255	0.084	0.197	0.888	0.063	0.084	1.035	85.8	
		Run 3	3.113	0.088	0.201	0.849	0.066	0.086	1.001	84.8	
		Run 4	2.810	0.089	0.238	0.766	0.067	0.102	0.935	82.0	
		Run 5	3.142	0.110	0.284	0.857	0.082	0.122	1.061	80.8	
		Run 6	2.305	0.068	0.194	0.629	0.051	0.083	0.763	82.4	

Table 7-4. Mass of each outlet gas, mass of carbon in each outlet gas, total mass of carbon in outlet gases, and CO_2 yield for each experiment run using torrefied wood at superficial velocities of 0.15 and 0.3 m/s under three bed configurations: no packing, RMSR, and ECA.

Velocity (m/s)	Packings	Experiments	CO2(g)	CH4(g)	CO(g)	C in CO2(g)	C in CH4 (g)	C in CO (g)	Total (g)	CO2 yield (%)	Avg CO2 yield (%)
0.15	No packing	Run 1	3.242	0.111	0.318	0.884	0.083	0.136	1.103	80.1	80.8
		Run 2	3.231	0.099	0.300	0.881	0.074	0.129	1.084	81.3	
		Run 3	2.848	0.089	0.267	0.777	0.067	0.114	0.958	81.1	
		Run 4	3.324	0.109	0.282	0.907	0.082	0.121	1.109	81.7	
		Run 5	3.085	0.106	0.310	0.841	0.080	0.133	1.054	79.8	
	RMSR	Run 1	3.667	0.065	0.056	1.000	0.049	0.024	1.073	93.2	93.7
		Run 2	3.809	0.067	0.054	1.039	0.050	0.023	1.112	93.4	
		Run 3	3.278	0.055	0.046	0.894	0.041	0.020	0.955	93.6	
		Run 4	4.138	0.066	0.050	1.129	0.050	0.021	1.200	94.1	
		Run 5	3.946	0.066	0.039	1.076	0.049	0.017	1.142	94.2	
	ECA	Run 1	3.746	0.066	0.065	1.022	0.050	0.028	1.099	92.9	93.1
		Run 2	3.382	0.059	0.057	0.922	0.045	0.024	0.991	93.1	
		Run 3	3.547	0.067	0.058	0.967	0.051	0.025	1.043	92.8	
		Run 4	3.515	0.057	0.063	0.959	0.043	0.027	1.029	93.2	
		Run 5	3.512	0.055	0.063	0.958	0.041	0.027	1.026	93.4	
0.3	No packing	Run 1	3.439	0.105	0.350	0.938	0.079	0.150	1.166	80.4	79.7
		Run 2	3.616	0.120	0.378	0.986	0.090	0.162	1.238	79.6	
		Run 3	3.352	0.110	0.363	0.914	0.083	0.155	1.152	79.3	
		Run 4	3.701	0.132	0.411	1.009	0.099	0.176	1.284	78.6	
		Run 5	3.439	0.105	0.350	0.938	0.079	0.150	1.166	80.4	
	RMSR	Run 1	4.083	0.100	0.113	1.114	0.075	0.049	1.237	90.0	91.4
		Run 2	4.219	0.090	0.093	1.151	0.067	0.040	1.258	91.5	
		Run 3	4.396	0.089	0.084	1.199	0.067	0.036	1.302	92.1	
		Run 4	4.373	0.086	0.088	1.193	0.065	0.038	1.295	92.1	
	ECA	Run 1	3.911	0.088	0.158	1.067	0.066	0.068	1.200	88.9	86.4
		Run 2	3.945	0.105	0.195	1.076	0.079	0.083	1.238	86.9	
		Run 3	3.780	0.099	0.153	1.031	0.074	0.065	1.171	88.1	
		Run 4	3.855	0.086	0.202	1.051	0.065	0.086	1.203	87.4	
		Run 5	3.458	0.094	0.236	0.943	0.070	0.101	1.114	84.6	
		Run 6	3.310	0.095	0.284	0.903	0.072	0.122	1.096	82.4	

Table 7-5. Average bed pressure for each experiment run using wood pellet at superficial velocities of 0.15 and 0.3 m/s under three bed configurations: no packing, RMSR, and ECA.

Velocity (m/s)	Packings	Experiments	Average pressure (kPa)
0.150	No packing	Run 1	7.999
		Run 2	7.960
		Run 3	7.994
		Run 4	7.989
	RMSR	Run 1	9.146
		Run 2	9.144
		Run 3	9.121
		Run 4	9.044
	ECA	Run 1	9.637
		Run 2	9.610
		Run 3	9.548
		Run 4	9.287
		Run 5	9.265
0.300	No packing	Run 1	8.829
		Run 2	8.782
		Run 3	8.789
	RMSR	Run 1	8.889
		Run 2	9.036
		Run 3	9.038
		Run 4	9.179
		Run 5	9.151
	ECA	Run 1	10.813
		Run 2	10.486
		Run 3	10.007
		Run 4	9.527
		Run 5	9.179
		Run 6	8.929

Table 7-6. Average bed pressure for each experiment run using torrefied wood at superficial velocities of 0.15 and 0.3 m/s under three bed configurations: no packing, RMSR, and ECA.

Velocity (m/s)	Packings	Experiments	Average pressure (kPa)
0.150	No packing	Run 1	7.570
		Run 2	7.552
		Run 3	7.548
		Run 4	7.557
		Run 5	7.535
	RMSR	Run 1	7.402
		Run 2	7.418
		Run 3	7.379
		Run 4	7.354
		Run 5	7.364
	ECA	Run 1	11.406
		Run 2	11.256
		Run 3	11.200
		Run 4	11.146
		Run 5	10.656
0.300	No packing	Run 1	9.322
		Run 2	9.301
		Run 3	9.235
		Run 4	9.231
		Run 5	9.245
	RMSR	Run 1	7.200
		Run 2	7.213
		Run 3	7.248
		Run 4	7.252
	ECA	Run 1	14.563
		Run 2	13.517
		Run 3	13.179
		Run 4	12.949
		Run 5	12.110
		Run 6	11.364

DEPARTMENT OF ENVIRONMENTAL AND ENERGY SCIENCES
CHALMERS UNIVERSITY OF TECHNOLOGY
Gothenburg, Sweden 2026
www.chalmers.se

CHALMERS
UNIVERSITY OF TECHNOLOGY